

Anyon-Induced Criticality and Dynamical Stability in Non-Hermitian Many-Body Systems

Yi Qin,¹ Yee Sin Ang,¹ Linhu Li,^{2,*} and Ching Hua Lee^{3,†}

¹*Science, Mathematics and Technology, Singapore University of Technology and Design, Singapore 487372, Singapore*

²*Quantum Science Center of Guangdong-Hong Kong-Macao Greater Bay Area (Guangdong), Shenzhen, China*

³*Department of Physics, National University of Singapore, Singapore 117542*

We show that anyonic statistics fundamentally reshapes non-Hermitian many-body physics by intrinsically breaking pseudo-Hermiticity, leading to a unique real-complex spectral transition with characteristically dense states in $\text{Im}E$. This anyon-induced transition occurs even when bosonic and pseudofermionic counterparts remain entirely real, revealing a form of non-Hermitian criticality driven purely by exchange statistics. The resulting spectrum exhibits enhanced gaps in $\text{Im}E$ that dynamically isolate dominant eigenstates, producing anomalously stable short-time quench dynamics for anyons. Our results identify anyonic statistics as an intrinsic mechanism for generating unconventional non-Hermitian critical behavior usually associated with highly non-local systems.

Introduction.— Abelian anyons, which interpolate continuously between bosons and fermions through a tunable statistical angle, have attracted longstanding interest as a fundamental extension of quantum statistics [1–18]. They play an essential role in understanding fractional quantum Hall physics and quantum computation [19–26]. Recent experimental breakthroughs in ultracold atomic systems have successfully engineered Abelian anyons and observed their characteristic asymmetric spreading dynamics [18, 27], paving the way for controlled studies of exotic quantum statistics in synthetic matter.

In parallel, non-Hermitian physics has emerged as a powerful framework to describe open quantum systems with gain and loss, leading to unique phenomena absent in Hermitian settings. Among these, the non-Hermitian skin effect (NHSE) [28–36] — the extensive localization of all bulk states at system boundaries — has become a central topic of intense research for their unconventional responses [37–51] in both single-particle [52–77] and many-body contexts [78–85]. More recently, a new form of criticality across the NHSE-deformed complex momentum solutions – the critical skin effect (CSE) – has been identified as a source of system size-dependent scale-free localization, fundamentally rooted in the competition between multiple NHSE localization channels [86–98].

In the many-body regime, the NHSE has led to even more sophisticated emergent phenomena [99–113], such as Fermi-like surfaces in real space and bosonic boundary condensation [80, 102–104, 114], with the latter being strongly suppressed by repulsive interactions [101, 105]. Rich classes of new many-body CSE states have also been identified in multi-component bosonic systems [115]. However, the interplay between anyonic statistics and non-Hermitian physics has scarcely been explored, particularly in the presence of nonlocal couplings that substantially enhance the significance of anyonic statistical phases.

In this Letter, we reveal a new type of critical phenomena fundamentally rooted in the anyonic statistics of coupled Abelian anyonic systems. Namely, anyonic statistics open up effectively nonlocal interacting channels that substantially alter the spectral structure, spontaneously breaking the pseudo-Hermiticity of the system, such as to allow an infinitesimal hopping perturbation to induce a real-complex spectral transition in the thermodynamic limit. In contrast to many-body CSE that relies on the order of hopping processes between scattering and/or bound states, such anyon-induced spectral transitions (AISTs) remains robust across different mixtures of these states, unveiling an emergent criticality insensitive to the explicit particle configurations. Furthermore, the anyonic statistics also reshape the broad structure of the imaginary spectrum, leading to an experimentally salient enhanced stability of the short-time quench dynamics.

Model for interacting 1D anyons.— Our study focuses on one-dimensional abelian anyons satisfying the commutation relations

$$\begin{aligned} [\hat{a}_j, \hat{a}_k]_\theta &\equiv \hat{a}_j \hat{a}_k - e^{-i\theta \text{sgn}(j-k)} \hat{a}_k \hat{a}_j = 0, \\ [\hat{a}_j, \hat{a}_k^\dagger]_{-\theta} &\equiv \hat{a}_j \hat{a}_k^\dagger - e^{i\theta \text{sgn}(j-k)} \hat{a}_k^\dagger \hat{a}_j = \delta_{jk}, \end{aligned} \quad (1)$$

with \hat{a}_j^\dagger the particle creation operator. The particles become bosons when $\theta = 0$ and pseudo-fermions when $\theta = \pi$ [12, 17]. To generate non-Hermitian interacting skin channels subject to emergent nonlocal hoppings, we consider a ladder consisting of A and B sublattices with Hubbard onsite interaction, described by the Hamiltonian $\hat{H} = \sum_{\sigma=A,B} \hat{H}_\sigma + \hat{H}_{AB} + \hat{H}_{\text{onsite}}$, with

$$\hat{H}_\sigma = -J \sum_{j=1}^{L-1} \left(e^{\alpha\sigma} \hat{a}_{j,\sigma}^\dagger \hat{a}_{j+1,\sigma} + e^{-\alpha\sigma} \hat{a}_{j+1,\sigma}^\dagger \hat{a}_{j,\sigma} \right), \quad (2)$$

$$\hat{H}_{AB} = J_p \sum_{j=1}^L \left(\hat{a}_{j,A}^\dagger \hat{a}_{j,B} + \hat{a}_{j,B}^\dagger \hat{a}_{j,A} \right), \quad (3)$$

$$\hat{H}_{\text{onsite}} = \frac{U}{2} \sum_{j=1,\sigma}^L \hat{n}_{j,\sigma} (\hat{n}_{j,\sigma} - 1) + \mu \sum_{j=1}^L (\hat{n}_{j,A} - \hat{n}_{j,B}). \quad (4)$$

Here $\sigma = A, B$ labels the two sublattices. The asymmetric hopping amplitudes $J e^{\pm\alpha\sigma}$ introduce non-reciprocity,

* lilinhu@quantumsc.cn

† phylch@nus.edu.sg

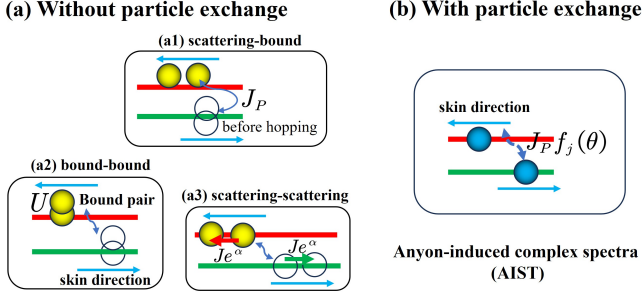


FIG. 1. Schematic illustration of representative interaction processes underlying the anyon-induced real-complex spectral transition (AIST) in coupled Abelian anyonic systems. (a) Processes without particle exchange: (a1) a scattering-bound process that hybridizes extended and bound two-particle configurations, (a2) a bound-bound process that renormalizes the bound-state sector, and (a3) a scattering-scattering process that reshapes the scattering continuum. These channels are determined by the composition of scattering and bound states and do not explicitly depend on the statistical angle θ . (b) Process with particle exchange, in which interchain hopping acquires an occupation-dependent Peierls phase $f_j(\theta)$. This exchange-enabled statistical channel introduces a θ -dependent asymmetry, breaks pseudo-Hermiticity, and can drive the emergence of AIST.

with $\alpha_{A/B} = \pm\alpha$, while J_P in \hat{H}_{AB} describes inter-sublattice hybridization. The onsite term \hat{H}_{onsite} includes the Hubbard interaction U and a staggered chemical potential $\pm\mu$ with $\hat{n}_{j,\sigma} = \hat{a}_{j,\sigma}^\dagger \hat{a}_{j,\sigma}$. Using a generalized Jordan–Wigner transformation (see supplemental Sec. I) [17, 113, 116],

$$\hat{a}_j = \hat{b}_j \exp\left(-i\theta \sum_{k=1}^{j-1} \hat{n}_k\right), \quad (5)$$

the anyonic Hamiltonian is mapped onto an effective bosonic Hamiltonian $\hat{H}_{\text{eff}} = \sum_{\sigma=A,B} \hat{H}_{\sigma}^{\text{eff}} + \hat{H}_{AB}^{\text{eff}} + \hat{H}_{\text{onsite}}$. Its explicit expression takes the same form as in Eq. (2) to Eq. (4), only with hopping terms acquiring occupation-dependent Peierls phases, given by

$$\hat{a}_{j,\sigma}^\dagger \hat{a}_{j+1,\sigma} \rightarrow \hat{b}_j^\dagger \hat{b}_{j+1} e^{-i\theta \hat{n}_{j,\sigma}}, \quad \hat{a}_{j,B}^\dagger \hat{a}_{j,A} \rightarrow f_j(\theta) \hat{b}_{j,B}^\dagger \hat{b}_{j,A}$$

and their Hermitian conjugate, with $f_j(\theta) = e^{i\theta(\sum_{k=j}^L \hat{n}_{k,A} + \sum_{k=1}^{j-1} \hat{n}_{k,B})}$. Here the number operator satisfies $\hat{n}_{j,\sigma} = \hat{a}_{j,\sigma}^\dagger \hat{a}_{j,\sigma} = \hat{b}_{j,\sigma}^\dagger \hat{b}_{j,\sigma}$, and importantly the statistical angle θ is encoded in $\hat{H}_{\sigma}^{\text{eff}}$ and $\hat{H}_{AB}^{\text{eff}}$ as local and nonlocal hopping phases, respectively.

AIST and emergent criticality from anyonic statistics.— A clean instance of an anyon-induced spectral transition (AIST) is reported in Fig. 2(a), where we compare the numbers of eigenenergies with nonzero imaginary parts ($\text{Im}E > 10^{-7}$ numerical threshold) as θ varies. Saliiently, for anyons ($\theta \neq 0$ or π), exponentially smaller inter-sublattice coupling J_p can already induce

complex eigenenergies and thus amplification. Interestingly, anyons exhibit not one but two onsets of complex spectra due to the coexistence of different orders of hopping processes between Fock states, as evident in the double plateau in Fig. 2(a) (see Supplemental Material Sects. II and III). In the following we shall focus only on the transition that leads to the first plateau.

To understand the origin of AIST, note that the Hamiltonian terms \hat{H}_{σ} and \hat{H}_{onsite} satisfy a pseudo-Hermitian symmetry that ensures real eigenenergies in its unbroken phase (see supplemental Sec. III),

$$\mathcal{K}(\hat{H}_{\sigma}^{\text{eff}} + \hat{H}_{\text{onsite}})\mathcal{K}^\dagger = (\hat{H}_{\sigma}^{\text{eff}} + \hat{H}_{\text{onsite}})^\dagger, \quad (6)$$

with $\mathcal{K} = \mathcal{R}_z \mathcal{I} \mathcal{T}$, \mathcal{I} the spatial inversion operator, \mathcal{T} the time-reversal operator, and $\mathcal{R}_z = \exp\left(-i\theta \sum_j \sum_{\sigma} \hat{n}_{j,\sigma} (\hat{n}_{j,\sigma} - 1)/2\right)$ a density-dependent phase rotation. However, the inter-sublattice term $\hat{H}_{AB}^{\text{eff}}$ breaks the \mathcal{K} -symmetry,

$$\mathcal{K} \hat{H}_{AB}^{\text{eff}} \mathcal{K}^\dagger \neq (\hat{H}_{AB}^{\text{eff}})^\dagger, \quad (7)$$

leading to complex eigenenergies when J_p cannot be ignored. The only exceptions are $\theta = 0$ and π , where the pseudo-Hermitian symmetry is restored for the full Hamiltonian, eliminating the real-complex energy transition unique to anyonic statistics.

Consistent with the above analysis, in Fig. 2(a), the system with $\theta = 0$ or π does not support complex eigenenergies until $J_p \gtrsim 10^{-2}$, which indicates a symmetry-breaking scenario accompanied with many-body CSEs, originating from interference between different many-body states [Fig. 1(a)]. Specifically for the chosen parameters, a mixed many-body bosonic CSE emerges from the interference between different scattering and bound states mixed in real energy, as shown in Figs. 2(a1) and 2(a2). On the other hand, anyonic statistic invalidates the \mathcal{K} -symmetry and induces complex eigenenergies at an exponentially smaller J_p for $\theta \neq 0, \pi$, resulting in complex eigenenergies dominating in both their numbers and imaginary magnitudes compared to the mixed many-body CSE, as can be seen from Figs. 2(a3) and 2(a4).

More generally, the AIST is still discernable even with weaker interaction strength U and onsite energy μ [Figs. 2(b)], where the system supports many-body CSEs from the interference between the same type of energy clusters [bound or scattering ones, see Figs. 2(b1) and (b2) for an example for bosons]. Similarly to the previous case [Figs. 2(a)], anyonic statistics enhances the sensitivity of the system, generating more complex eigenenergies at a smaller J_p . Nevertheless, note that the mixed many-body CSE involves hopping processes that break the interaction-bound pairs of particles to form scattering states. In contrast, the scattering many-body CSE involves only scattering states, thus it is much more significant and may overwhelm the AIST under relatively stronger J_p , as shown in Fig. 2(b4).

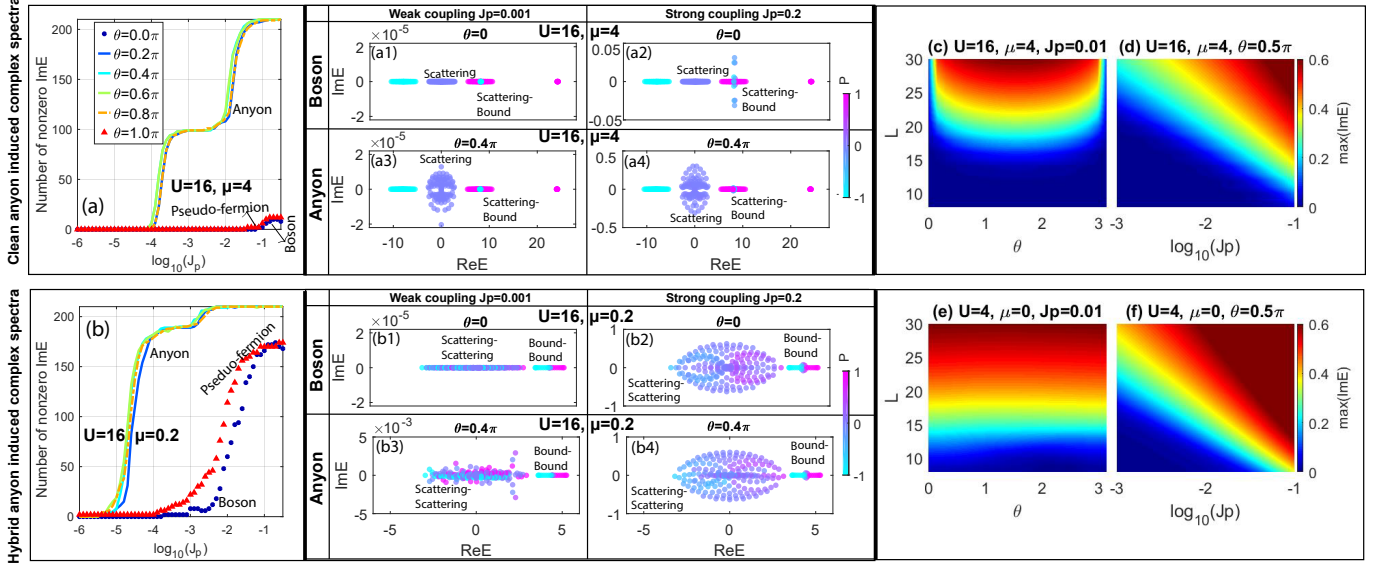


FIG. 2. **Clean (Top Row) and Hybrid (Bottom Row) anyon-induced real-complex transition (AIST) for two particles.** Anyons, unlike bosons ($\theta = 0$) and pseudofermions ($\theta = \pi$), generically undergo a real-complex transition already in the scattering subspace at small J_p . (a) Number of eigenstates with nonzero imaginary energies ($\text{Im}E > 10^{-7}$ in numerics) as a function of J_p , with $U = 16$, $\mu = 4$. Compared with bosons ($\theta = 0$) and pseudofermions ($\theta = \pi$), anyons acquire complex eigenenergies at an exponentially smaller J_p . (a1) to (a4) show representative spectra colored by the sublattice polarization $P = (N_A - N_B)/(N_A + N_B)$, with $N_\sigma = \sum_x \langle \hat{n}_{x,\sigma} \rangle$. The mixture of scattering and bound states lead to the mixed many-body CSE that generates complex eigenenergies under a weak J_p [(a1) and (a2)], which are dominated by those from AIST in both their numbers and magnitudes [(a3) and (a4)]. (b) and (b1) to (b4) show the same quantities as (a) and (a1) to (a4), but with different interaction and on-site potential $U = 4$, $\mu = 0.2$. Scattering and bound states are now separated in real energy. The resultant AIST and many-body CSE are qualitatively similar, except that the scatter many-body CSE overwhelms the AIST under a relatively strong J_p in (b4). (c) and (d) Maximum imaginary eigenenergy, $\text{Max}(\text{Im}E)$, for $U = 16$ and $\mu = 4$ as in (a). In (c), AIST is clearly recognized by zero and nonzero $\text{Max}(\text{Im}E)$ with $\theta = 0, \pi$ and generic θ as L increases, respectively. Its critical nature can be identified in (d) by the threshold of J_p to induce nonzero $\text{Max}(\text{Im}E)$, which approaches zero exponentially as the system size L increases. (e) and (f) the same as (c) and (d), but with $U = 4$ and $\mu = 0$ as in (b). The scattering many-body CSE dominates the complex eigenvalues, leading similar $\text{Max}(\text{Im}E)$ for arbitrary θ values in (e). In (f), the threshold of J_p also decreases exponentially as L increases. Other parameters are $J = e^\alpha = 1/\sqrt{2}$ and $L = 10$, unless otherwise specified.

To clarify the interplay between the AIST and the many-body CSE, in Figs. 2(c) to 2(f) we demonstrate the maximal $\text{Im}E$ versus θ , J_p , and L , for the previous two representative choices of U and μ . In Fig. 2(c) with large μ and strong U , the maximum $\text{Im}E$ jumps from zero to a finite value as θ deviates from 0 and π , signaling a statistics-driven criticality from the AIST that overwhelms the mixed many-body CSE in this parameter regime. In contrast, scattering many-body CSE in the regime with weaker U and μ becomes the main origin of complex eigenenergies, resulting in similar maximum $\text{Im}E$ for different θ , as shown in Fig. 2(e). Nevertheless, as can be seen in Figs. 2(d) and 2(f), the threshold of J_p to induce complex eigenenergies in both cases tends to zero as L approaches infinity, unveiling qualitatively the same criticality for many-body CSE and AIST, despite that they origin from different symmetry-breaking or -invalidation mechanisms.

Anyon-enhanced imaginary spectral density of states.— The emergent long-ranged nature of non-Hermitian anyonic interactions also manifest as unconventionally high

density of states along the $\text{Im}E$ direction, as shown in Fig. 3 (a,b) vs. (c,d). This has far-reaching dynamical consequences which will be discussed later.

For bosons and pseudofermions [Figs. 3(a) and 3(b)], most eigenenergies remains real, with a few acquiring nonzero $\text{Im}E$ as the coupling J_p increases. Notably, these imaginary energies cross each other at certain J_p , swapping the maximum- $\text{Im}E$ state that dominates the long-time dynamics before and after the crossing. Such distinct swapping of maximal $\text{Im}E$ results in a sharp discontinuity in the first derivative (top of each panel). Meanwhile, imaginary gaps between different energies remain small.

In contrast, macroscopically many anyonic eigenstates possess large $\text{Im}E$ due to the sustained non-local feedback from the statistical angle θ . The swapping of maximal $\text{Im}E$ is comparably less clear, but can also be identified by a slight qualitatively distinct discontinuity in the derivative.

Note that imaginary eigenenergies arise from the non-negligible effect of J_p , which couples the two sublattices.

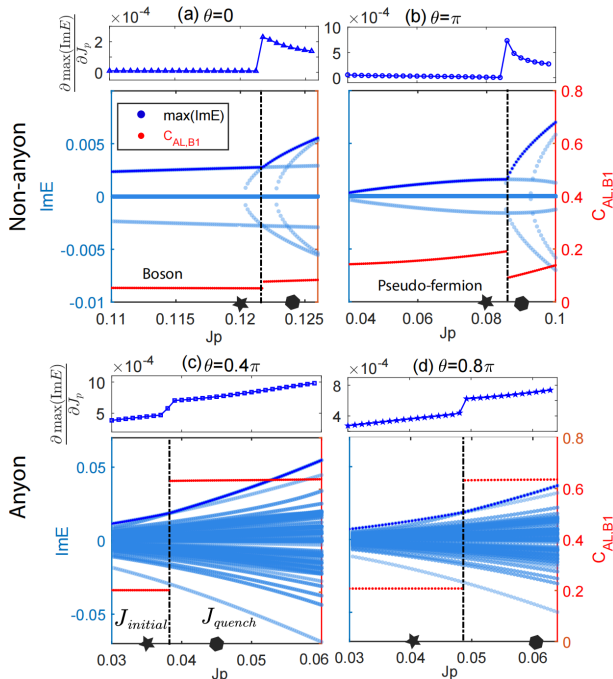


FIG. 3. **Qualitatively distinct imaginary density of states and spectral transitions between anyonic and non-anyonic systems.** Unlike bosons and pseudofermions, generic anyons exhibit broadly complex spectra, indicating pseudo-Hermiticity breaking via AIST. (a) and (b) imaginary spectrum (blue) versus J_p for bosons and pseudofermions, respectively. Discontinuous jumps of eigenenergies from real to complex values signal the breaking of pseudo-Hermiticity for eigenstates in the many-body CSE. A transition of $\text{Max}(\text{Im}E)$ (dark blue) is clearly seen in either case, where two states cross each other in $\text{Im}E$ (vertical dashed line). Top panels show the first derivative of $\text{Max}(\text{Im}E)$, which jumps discontinuously at the transition point. (c) and (d) the same as (a) and (b), but for anyons with different θ values. Eigenenergies generally take complex values, indicating the invalidation of pseudo-Hermiticity for the Hamiltonian corresponding to AIST. The imaginary-energy spacing becomes much smaller, yet the transition of $\text{Max}(\text{Im}E)$ still persists, as can be seen from the discontinuous change of its derivative. The transition is also marked by the jump of the edge correlation $C_{AL,B1}$ of the state with maximum $\text{Im}E$ (red dots). The imaginary energy distribution and its response to coupling differ markedly between anyonic and non-anyonic systems. Other parameters are $U = 16$, $\mu = 4$, and, $L = 10$, $J = e^\alpha = 1/\sqrt{2}$. black stars and hexagons mark the parameters before and after quench is Fig. 4.

tices A and B with rightward and leftward non-reciprocal pumping, respectively. This tendency is captured by the boundary correlation function

$$C_{AL,B1} = \langle \phi | \hat{n}_{A,L} \hat{n}_{B,1} | \phi \rangle \quad (8)$$

which measures the density–density correlation between the last site of sublattice A and the first site of sublattice B for the maximum- $\text{Im}E$ state $|\phi\rangle$. As shown in the red dashed curves in Fig. 3, $C_{AL,B1}$ jumps abruptly when

the maximum $\text{Im}E$ state switches. Surprisingly, despite the anyonic case exhibiting a much less noticeable change in $\text{Im}E$ gradient, its $C_{AL,B1}$ can jump very dramatically, suggestive of non-local state transitions beyond what is perceptible through spectral transitions alone.

Anyon-induced stabilization of quench dynamics.— To elucidate the dynamical consequences of the above-mentioned proliferation of imaginary eigenenergies for anyons, we consider a quench across two coupling parameter values J_{ini} and J_{final} chosen across the maximum- $\text{Im}E$ state transitions in Fig. 3, marked by the black stars and hexagons:

$$\begin{cases} t = 0 : & J_p = J_{\text{ini}}, \\ t > 0 : & J_p = J_{\text{final}}, \end{cases} \quad (9)$$

where the system is initialized in the maximum-imaginary-energy eigenstate $|\psi_{\text{ini}}\rangle$ of $H(J_{\text{ini}})$ and then evolving as

$$|\psi(t)\rangle = \frac{e^{-iH(J_{\text{final}})t} |\psi_{\text{ini}}\rangle}{\sqrt{\langle \psi_{\text{ini}} | e^{+iH^\dagger(J_{\text{final}})t} e^{-iH(J_{\text{final}})t} | \psi_{\text{ini}} \rangle}}. \quad (10)$$

In Fig. 4(a), anyons are seen to have very stable boundary correlation in their short-time dynamics, suggesting the domination of the pre-quench state $|\psi_{\text{ini}}\rangle$ due to the anyonic spectral feature. That is, the pre-quench and after-quench maximal- $\text{Im}E$ states have close imaginary energies separated from the rest [see Figs. 3(c) and 3(d)], allowing the former to persist during a certain period of time. The dynamically stable regime can be estimated by a two-state approximation, $|\psi(t)\rangle \approx c_0 e^{-iE_0 t} |\psi_0\rangle + c_1 e^{-iE_1 t} |\psi_1\rangle$, with $|\psi_{0,1}\rangle$ the after-quench states with maximal and second-maximal $\text{Im}E$, and $E_{0,1}$ the corresponding eigenenergies. At time t , their relative weight evolves as $\frac{|c_0(t)|}{|c_1(t)|} = \frac{|c_0|}{|c_1|} e^{(\text{Im}E_0 - \text{Im}E_1)t}$, leading to a crossover at $t_c = \frac{\ln(|c_0/c_1|)}{\text{Im}E_1 - \text{Im}E_0} \sim 10^3$, consistent with our observation.

In addition, we note that the maximal imaginary energy has a two-fold degeneracy, resulting in a strong oscillation in the long-time dynamics [see the inset of Fig. 4(a) and supplemental Sec. IV]. In contrast, bosons and pseudofermions have a sparse imaginary spectrum with small gaps between different eigenstates [see Figs. 3(a) and 3(b)]. Therefore, more eigenstates participate in the short-time dynamics, leading to strong fluctuations in the boundary correlation (see supplemental Sec. V).

The stability of anyonic dynamics is further apparent in their fidelity evolution, quantified by the normalized overlap function between the initial and final states,

$$P(t) = |\langle \psi(t) | \psi_{\text{ini}} \rangle|. \quad (11)$$

As in Fig. 4(b), $P(t) \approx 1$ for anyons across an extended initial period, reflecting the domination of $|\psi_{\text{ini}}\rangle$ in the short-time dynamics; while bosons and pseudofermions show an oscillated dynamics with contributions from multiple states. Finally, we note that the dynamical behaviors discussed above are qualitatively the same

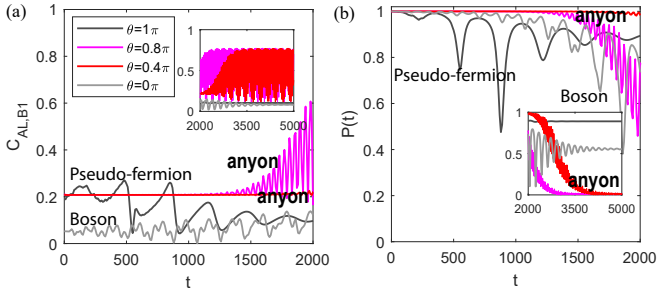


FIG. 4. **Dynamical stability induced by anyonic statistics.** (a) and (b) boundary correlation $C_{AL,B1}(t)$ of the final state and its overlap with the initial state $P(t)$, respectively. The pre- and post-quenched parameters are $(J_{\text{ini}}, J_{\text{final}}) = (0.12, 0.124)$ for $\theta = 0$, $(0.035, 0.045)$ for 0.4π , $(0.04, 0.06)$ for 0.8π , and $(0.08, 0.09)$ for π , as marked by black stars and hexagons in Fig. 3. In the short-time regime (approximately with $t < 10^3$), bosons and pseudofermions show strong fluctuations in the demonstrated quantities, while anyons are dynamically stable after quenching. Beyond this regime, anyons exhibit strong oscillations in $C_{AL,B1}(t)$ as their maximal $\text{Im}E$ are two-fold degenerate (see supplemental Sec. IV). Other parameters are $N = 2$, $U = 16$, $\mu = 4$, $L = 10$, and $J = e^\alpha = 1/\sqrt{2}$.

for different hopping parameters and anyonic phases, as demonstrated in Supplemental Materials Sec. VI and VII.

Conclusion.— We uncover emergent criticality induced by anyonic statistics in a non-Hermitian anyonic system, marked by a transition towards a spectrum that is dense in the $\text{Im}E$ axis. This phenomenon also highlights the crucial role of the effective nonlocal hopping that emerges in the bosonic representation of the anyonic system, where it carries a string of phases set by the particle occupations throughout the system. Although the main

text focuses on the two-particle sector for clarity, the robustness of the AIST and the associated critical behavior *persists* in higher-particle sectors, as demonstrated in Supplemental Material Sec. IV. Beyond inducing criticality, anyonic statistics is also found to fundamentally reshape the structure of the imaginary spectrum, leading to stabilized short-time dynamics in quantum quench.

We emphasize that the AIST is fundamentally distinct from the real-complex transition in the many-body CSE, which originate from the feedback amplification among different coupled NHSE channels, analogous to the single-particle CSE. The AIST, in contrast, generates complex eigenenergies due to the emergent non-locality from the statistical phase itself, which operates exclusively in the many-body scenario. The resulting transition and criticality therefore constitute an intrinsic many-body phenomenon with no single-particle counterpart. Experimentally, the predicted non-Hermitian phenomenon may be realized in universal digital quantum simulators [43, 84, 114, 117–121] and in particular ultracold-atom platforms, where non-Hermiticity and Abelian anyonic statistics [18, 27] have recently been engineered in distinct setups, opening a viable route toward observing the AIST and its associated dynamical signatures.

Acknowledgements.— L. L. is supported by the National Natural Science Foundation of China (Grant No. 12474159) and the Guangdong Provincial Quantum Science Strategic Initiative (Grant No. GDZX2504003 and No. GDZX2504006). Y. S. A. is supported by the Kwan Im Thong Hood Cho Temple Early Career Chair Professorship and the Singapore Ministry of Education Academic Research Fund (AcRF) Tier 2 Grant under the award number T2EP50125-0015. C.H.L. and Y.Q. acknowledges support from the Singapore Ministry of Education Tier II grants MOE-T2EP50224-0007 and MOE-T2EP50224-0021 (WBS nos. A-8003505-01-00 and A-8003910-00-00).

-
- [1] Frank Wilczek, “Magnetic flux, angular momentum, and statistics,” *Phys. Rev. Lett.* **48**, 1144–1146 (1982).
- [2] D. C. Tsui, H. L. Stormer, and A. C. Gossard, “Two-dimensional magnetotransport in the extreme quantum limit,” *Phys. Rev. Lett.* **48**, 1559–1562 (1982).
- [3] R. B. Laughlin, “Anomalous quantum hall effect: An incompressible quantum fluid with fractionally charged excitations,” *Phys. Rev. Lett.* **50**, 1395–1398 (1983).
- [4] Yajiang Hao, Yumbo Zhang, and Shu Chen, “Ground-state properties of one-dimensional anyon gases,” *Physical Review A—Atomic, Molecular, and Optical Physics* **78**, 023631 (2008).
- [5] Yajiang Hao, Yumbo Zhang, and Shu Chen, “Ground-state properties of hard-core anyons in one-dimensional optical lattices,” *Physical Review A—Atomic, Molecular, and Optical Physics* **79**, 043633 (2009).
- [6] Yajiang Hao and Shu Chen, “Dynamical properties of hard-core anyons in one-dimensional optical lattices,” *Physical Review A—Atomic, Molecular, and Optical Physics* **86**, 043631 (2012).
- [7] B. I. Halperin, “Statistics of quasiparticles and the hierarchy of fractional quantized hall states,” *Phys. Rev. Lett.* **52**, 1583–1586 (1984).
- [8] Daniel Arovas, J. R. Schrieffer, and Frank Wilczek, “Fractional statistics and the quantum hall effect,” *Phys. Rev. Lett.* **53**, 722–723 (1984).
- [9] Hong Yao and Steven A. Kivelson, “Exact chiral spin liquid with non-abelian anyons,” *Phys. Rev. Lett.* **99**, 247203 (2007).
- [10] B. Bauer, L. Cincio, B. P. Keller, M. Dolfi, G. Vidal, S. Trebst, and A. W. W. Ludwig, “Chiral spin liquid and emergent anyons in a kagome lattice mott insulator,” *Nat. Commun.* **5**, 5137 (2014).
- [11] Alexei Kitaev, “Anyons in an exactly solved model and beyond,” *Annals of Physics* **321**, 2–111 (2006).
- [12] Tassilo Keilmann, Simon Lanzmich, Ian McCulloch, and Marco Roncaglia, “Statistically induced phase transitions and anyons in 1d optical lattices,” *Nature communications*

- 2, 361 (2011).
- [13] Sebastian Greschner and Luis Santos, “Anyon hubbard model in one-dimensional optical lattices,” *Phys. Rev. Lett.* **115**, 053002 (2015).
- [14] J. Arcila-Forero, R. Franco, and J. Silva-Valencia, “Critical points of the anyon-hubbard model,” *Phys. Rev. A* **94**, 013611 (2016).
- [15] J. Arcila-Forero, R. Franco, and J. Silva-Valencia, “Three-body-interaction effects on the ground state of one-dimensional anyons,” *Phys. Rev. A* **97**, 023631 (2018).
- [16] Florian Lange, Satoshi Ejima, and Holger Fehske, “Anyonic haldane insulator in one dimension,” *Phys. Rev. Lett.* **118**, 120401 (2017).
- [17] Fangli Liu, James R. Garrison, Dong-Ling Deng, Zhe-Xuan Gong, and Alexey V. Gorshkov, “Asymmetric particle transport and light-cone dynamics induced by anyonic statistics,” *Phys. Rev. Lett.* **121**, 250404 (2018).
- [18] Joyce Kwan, Perrin Segura, Yanfei Li, Sooshin Kim, Alexey V. Gorshkov, André Eckardt, Brice Bakkali-Hassani, and Markus Greiner, “Realization of one-dimensional anyons with arbitrary statistical phase,” *Science* **386**, 1055–1060 (2024), <https://www.science.org/doi/pdf/10.1126/science.adi3252>.
- [19] A Yu Kitaev, “Fault-tolerant quantum computation by anyons,” *Annals of physics* **303**, 2–30 (2003).
- [20] Sankar Das Sarma, Michael Freedman, and Chetan Nayak, “Topologically protected qubits from a possible non-abelian fractional quantum hall state,” *Phys. Rev. Lett.* **94**, 166802 (2005).
- [21] Chetan Nayak, Steven H. Simon, Ady Stern, Michael Freedman, and Sankar Das Sarma, “Non-abelian anyons and topological quantum computation,” *Rev. Mod. Phys.* **80**, 1083–1159 (2008).
- [22] Matteo Carrega, Luca Chirolli, Stefan Heun, and Lucia Sorba, “Anyons in quantum hall interferometry,” *Nature Reviews Physics* **3**, 698–711 (2021).
- [23] Mohsin Iqbal, Nathanan Tantivasadakarn, Ruben Verresen, Sara L Campbell, Joan M Dreiling, Caroline Figgatt, John P Gaebler, Jacob Johansen, Michael Mills, Steven A Moses, *et al.*, “Non-abelian topological order and anyons on a trapped-ion processor,” *Nature* **626**, 505–511 (2024).
- [24] June-Young M Lee, Changki Hong, Tomer Alkalay, Noam Schiller, Vladimir Umansky, Moty Heiblum, Yuval Oreg, and H-S Sim, “Partitioning of diluted anyons reveals their braiding statistics,” *Nature* **617**, 277–281 (2023).
- [25] Ching Hua Lee, Zlatko Papić, and Ronny Thomale, “Geometric construction of quantum hall clustering hamiltonians,” *Phys. Rev. X* **5**, 041003 (2015).
- [26] Ching Hua Lee, Wen Wei Ho, Bo Yang, Jiangbin Gong, and Zlatko Papić, “Floquet mechanism for non-abelian fractional quantum hall states,” *Phys. Rev. Lett.* **121**, 237401 (2018).
- [27] Sudipta Dhar, Botao Wang, Milena Horvath, Amit Vashisht, Yi Zeng, Mikhail B Zvonarev, Nathan Goldman, Yanliang Guo, Manuele Landini, and Hanns-Christoph Nägerl, “Observing anyonization of bosons in a quantum gas,” *Nature* **642**, 53–57 (2025).
- [28] Shunyu Yao and Zhong Wang, “Edge states and topological invariants of non-hermitian systems,” *Phys. Rev. Lett.* **121**, 086803 (2018).
- [29] Shunyu Yao, Fei Song, and Zhong Wang, “Non-hermitian chern bands,” *Phys. Rev. Lett.* **121**, 136802 (2018).
- [30] V. M. Martinez Alvarez, J. E. Barrios Vargas, and L. E. F. Foa Torres, “Non-hermitian robust edge states in one dimension: Anomalous localization and eigenspace condensation at exceptional points,” *Phys. Rev. B* **97**, 121401 (2018).
- [31] Ching Hua Lee and Ronny Thomale, “Anatomy of skin modes and topology in non-hermitian systems,” *Phys. Rev. B* **99**, 201103 (2019).
- [32] Nobuyuki Okuma and Masatoshi Sato, “Non-hermitian topological phenomena: A review,” *Annual Review of Condensed Matter Physics* **14**, 83–107 (2023).
- [33] Xiujuan Zhang, Tian Zhang, Ming-Hui Lu, and Yan-Feng Chen, “A review on non-hermitian skin effect,” *Advances in Physics: X* **7**, 2109431 (2022).
- [34] Rijia Lin, Tommy Tai, Linhu Li, and Ching Hua Lee, “Topological non-hermitian skin effect,” *Frontiers of Physics* **18**, 53605 (2023).
- [35] Julius T Gohsrich, Ayan Banerjee, and Flore K Kunst, “The non-hermitian skin effect: A perspective,” *Europhysics Letters* **150**, 60001 (2025).
- [36] Xianquan Yan, Hakan Akgün, Kenji Kawaguchi, N Duane Loh, and Ching Hua Lee, “Hsg-12m: A large-scale spatial multigraph dataset,” *arXiv preprint arXiv:2506.08618* (2025).
- [37] Fang Qin, Ruizhe Shen, Linhu Li, and Ching Hua Lee, “Kinked linear response from non-hermitian cold-atom pumping,” *Phys. Rev. A* **109**, 053311 (2024).
- [38] Juntao Huang, Jiangping Hu, and Zhesen Yang, “Complex frequency detection in a subsystem,” *Communications Physics* **9**, 84 (2026).
- [39] Yifei Yi and Zhesen Yang, “Anomalous scaling behavior of green’s function in critical skin effects,” *Phys. Rev. B* **112**, 174303 (2025).
- [40] Yufei Zhao, Kai Zhang, Jiewen Xiao, Kai Sun, and Binghai Yan, “Magnetochiral charge pumping due to charge trapping and skin effect in chirality-induced spin selectivity,” *Nature communications* **16**, 37 (2025).
- [41] Ruizhe Shen, Tianqi Chen, Mohammad Mujahid Aliyu, Fang Qin, Yin Zhong, Huanqian Loh, and Ching Hua Lee, “Proposal for observing yang-lee criticality in rydberg atomic arrays,” *Physical Review Letters* **131**, 080403 (2023).
- [42] Bo Li, Chuan Chen, and Zhong Wang, “Universal non-hermitian transport in disordered systems,” *Phys. Rev. Lett.* **135**, 033802 (2025).
- [43] Lei Xiao, Wen-Tan Xue, Fei Song, Yu-Min Hu, Wei Yi, Zhong Wang, and Peng Xue, “Observation of non-hermitian edge burst in quantum dynamics,” *Phys. Rev. Lett.* **133**, 070801 (2024).
- [44] Shulin Wang, Bing Wang, Chenyu Liu, Chengzhi Qin, Lange Zhao, Weiwei Liu, Stefano Longhi, and Peixiang Lu, “Nonlinear non-hermitian skin effect and skin solitons in temporal photonic feedforward lattices,” *Physical Review Letters* **134**, 243805 (2025).
- [45] Wenquan Wu, Qicheng Zhang, Liangjun Qi, Kun Zhang, Shuaishuai Tong, and Chunyin Qiu, “Observation of dislocation non-hermitian skin effect in a torus-like acoustic metamaterial,” *Advanced Materials* **38**, e14101 (2026).
- [46] Mengjie Yang and Ching Hua Lee, “Beyond the non-hermitian skin effect: Scaling-controlled topology from exceptional-bound bands,” *Advanced Science* , e23989 (2025).
- [47] Wen-Tan Xue, Fei Song, Yu-Min Hu, and Zhong Wang, “Non-bloch edge dynamics of non-hermitian lattices,” *arXiv preprint arXiv:2503.13671* (2025).

- [48] Mengjie Yang and Ching Hua Lee, “Reversing non-hermitian skin accumulation with a non-local transverse switch,” arXiv preprint arXiv:2509.02686 (2025).
- [49] Nobuyuki Okuma, “Steady-state skin effect in bosonic topological edge states under parametric driving,” (2026), arXiv:2602.01625 [cond-mat.mes-hall].
- [50] Xulong Wang, Dongyi Wang, Congwei Lu, Ruo-Yang Zhang, Ching Hua Lee, Kun Ding, and Guancong Ma, “Observation of flat-band skin effect,” arXiv preprint arXiv:2512.19745 (2025).
- [51] Letian Yu, Cesare Soci, YD Chong, and Baile Zhang, “Sensitivity evaluation for global perturbations in non-hermitian skin-effect sensors,” *Nanophotonics* **15**, e70039 (2026).
- [52] Nobuhiro Ito and Shun Uchino, “Edge-controlled non-hermitian skin effect in the modified haldane model,” (2026), arXiv:2603.01503 [cond-mat.mes-hall].
- [53] Heng Lin, Yunyao Qi, and Gui-Lu Long, “Global bifurcations and basin geometry of the nonlinear non-hermitian skin effect,” (2026), arXiv:2602.17439 [quant-ph].
- [54] S Rahul and Pasquale Marra, “Controlling energy spectra and skin effect via boundary conditions in non-hermitian lattices,” (2026), arXiv:2602.16780 [quant-ph].
- [55] Kazuma Saito, Ryo Okugawa, Kazuki Yokomizo, Takami Tohyama, and Chen-Hsuan Hsu, “Quasiperiodicity-induced non-hermitian skin effect from the breakdown of scale-free localization,” (2026), arXiv:2602.11155 [cond-mat.mes-hall].
- [56] J. N. Bai, F. Yang, D. Yan, Weibin Li, and X. Q. Shao, “Engineering the non-hermitian ssh model with skin effects in rydberg atom arrays,” (2026), arXiv:2601.20114 [quant-ph].
- [57] Xiaosen Yang, Yaru Feng, Abdul Wahab, and Hao Geng, “Non-hermitian second-order topological phases and bipolar skin effect in photonic kagome crystals,” *Phys. Rev. A* **113**, 023506 (2026).
- [58] Jien Wu, Yejian Hu, Zhaojian He, Ke Deng, Xueqin Huang, Manzhu Ke, Weiyin Deng, Jiuyang Lu, and Zhengyou Liu, “Hybrid-order skin effect from loss-induced nonreciprocity,” *Phys. Rev. Lett.* **134**, 176601 (2025).
- [59] Lingfang Li, Yating Wei, Gangzhou Wu, Yang Ruan, Shihua Chen, Ching Hua Lee, and Zhenhua Ni, “Exact solutions disentangle higher-order topology in two-dimensional non-hermitian lattices,” *Physical Review B* **111**, 075132 (2025).
- [60] Linhu Li and Ching Hua Lee, “Non-hermitian pseudogaps,” *Science Bulletin* **67**, 685–690 (2022).
- [61] Tian-Rui Liu, Tao Liu, and Meng Xiao, “Anomalous non-hermitian skin effect of chiral boundary states,” *Physical Review B* **112**, L081112 (2025).
- [62] Mingyang Li, Jing Lin, and Kun Ding, “Algebraic skin effect in two-dimensional non-hermitian metamaterials,” arXiv preprint arXiv:2501.13440 (2025).
- [63] SM Rafi-Ul-Islam, Zhuo Bin Siu, Haydar Sahin, Ching Hua Lee, and Mansoor BA Jalil, “Unconventional skin modes in generalized topoelectrical circuits with multiple asymmetric couplings,” *Physical Review Research* **4**, 043108 (2022).
- [64] Haiping Hu, “Topological origin of non-hermitian skin effect in higher dimensions and uniform spectra,” *Science Bulletin* **70**, 51–57 (2025).
- [65] Habib Ammari, Silvio Barandun, Jinghao Cao, Bryn Davies, Erik Orvehed Hiltunen, and Ping Liu, “The non-hermitian skin effect with three-dimensional long-range coupling,” *J. Eur. Math. Soc.(JEMS)* (2025).
- [66] Yu-Hong Han, Yi Li, Jia-Hui Zhang, Yang Kou, Liantuan Xiao, Suotang Jia, Linhu Li, and Feng Mei, “Observation of gauge field induced non-hermitian helical skin effects,” *Chinese Physics Letters* (2026).
- [67] Shan-Zhong Li, Linhu Li, Shi-Liang Zhu, and Zhi Li, “Anderson-skin dualism: A boundary-dependent effect in non-hermitian disordered coupled systems,” *Physical Review B* **112**, L201108 (2025).
- [68] Kai Zhang, Zhesen Yang, and Kai Sun, “Edge theory of non-hermitian skin modes in higher dimensions,” *Phys. Rev. B* **109**, 165127 (2024).
- [69] Kai Zhang, Chen Fang, and Zhesen Yang, “Dynamical degeneracy splitting and directional invisibility in non-hermitian systems,” *Phys. Rev. Lett.* **131**, 036402 (2023).
- [70] Yixuan Li, Linhu Li, and Zhihao Xu, “Size-dependent skin effect transitions in weakly coupled nonreciprocal chains,” *Phys. Rev. B* **112**, 235122 (2025).
- [71] Jingnan Yang, Yi Qin, Linhu Li, and Xiulai Xu, “Configurable localized states in non-hermitian extended schrieffer-heeger model,” *New Journal of Physics* **27**, 113001 (2025).
- [72] Zuxuan Ou, Hui-Qiang Liang, Guo-Fu Xu, and Linhu Li, “Anisotropic scaling localization in higher-dimensional non-hermitian systems,” *Phys. Rev. B* **112**, L161109 (2025).
- [73] Zhoutao Lei and Linhu Li, “Inter-species topological phases via a dynamical gauge field,” arXiv preprint arXiv:2504.05390 (2025).
- [74] He-Ran Wang, Bo Li, Fei Song, and Zhong Wang, “Scale-free non-Hermitian skin effect in a boundary-dissipated spin chain,” *SciPost Phys.* **15**, 191 (2023).
- [75] Kai Zhang, Chang Shu, and Kai Sun, “Algebraic non-hermitian skin effect and generalized fermi surface formula in arbitrary dimensions,” *Phys. Rev. X* **15**, 031039 (2025).
- [76] Chang Shu, Kai Zhang, and Kai Sun, “Ultraspectral sensitivity and nonlocal bound states in algebraic non-hermitian skin effect,” *Phys. Rev. B* **112**, 235152 (2025).
- [77] Qingya Li, Hui Jiang, and Ching Hua Lee, “Phase-space generalized brillouin zone for spatially inhomogeneous non-hermitian systems,” arXiv preprint arXiv:2501.09785 (2025).
- [78] Yue Wang, Xiangyu Zhang, Zhesen Yang, and Congjun Wu, “Explicit wave function of the interacting non-hermitian spin-1/2 1d system,” *Phys. Rev. Lett.* **136**, 036501 (2026).
- [79] Zichang Hao, Wei Jie Chan, and Ching Hua Lee, “Interacting many-body non-hermitian systems as markov chains,” arXiv preprint arXiv:2509.05411 (2025).
- [80] Mengjie Yang, Luqi Yuan, and Ching Hua Lee, “Non-hermitian strong bosonic clustering through interaction-induced caging,” *Communications Physics* **8**, 388 (2025).
- [81] Zhi Jiao Deng, Xing Yao Mi, Ruo Kun Cai, Chun Wang Wu, and Ping Xing Chen, “Confined non-hermitian skin effect in a semi-infinite fock-state lattice,” (2026), arXiv:2601.13540 [quant-ph].
- [82] Bin Yi, “Directional dynamics of the non-hermitian skin effect,” (2026), arXiv:2602.18106 [quant-ph].
- [83] Stefano Longhi, “Erratic liouvillian skin localization and subdiffusive transport,” (2026), arXiv:2602.14698 [quant-ph].
- [84] Jin Ming Koh, Wen-Tan Xue, Tommy Tai, Dax Enshan Koh, and Ching Hua Lee, “Interacting non-hermitian edge and cluster bursts on a digital quantum processor,”

- arXiv preprint arXiv:2503.14595 (2025).
- [85] Shu Long, Chao Yang, Sen Mu, and Linhu Li, “Symmetry-protected control of liouvillian topological phases via hamiltonian band topology,” (2026), arXiv:2602.22323 [quant-ph].
- [86] Linhu Li, Ching Hua Lee, Sen Mu, and Jiangbin Gong, “Critical non-hermitian skin effect,” *Nature Communications* **11** (2020), 10.1038/s41467-020-18917-4.
- [87] Yanxia Liu, Yumeng Zeng, Linhu Li, and Shu Chen, “Exact solution of the single impurity problem in non-reciprocal lattices: Impurity-induced size-dependent non-hermitian skin effect,” *Phys. Rev. B* **104**, 085401 (2021).
- [88] SM Rafi-Ul-Islam, Zhuo Bin Siu, Haydar Sahin, Ching Hua Lee, and Mansoor BA Jalil, “Critical hybridization of skin modes in coupled non-hermitian chains,” *Physical Review Research* **4**, 013243 (2022).
- [89] Hui-Qiang Liang, Linhu Li, and Guo-Fu Xu, “Size-dependent critical localization,” arXiv preprint arXiv:2509.18943 (2025).
- [90] SM Rafi-Ul-Islam, Zhuo Bin Siu, Md Saddam Hossain Razo, and Mansoor BA Jalil, “Critical non-hermitian skin effect in a cross-coupled hermitian chain,” *Physical Review B* **111**, 115415 (2025).
- [91] Mengjie Yang and Ching Hua Lee, “Percolation-induced pt symmetry breaking,” *Physical Review Letters* **133**, 136602 (2024).
- [92] Yu Zhang, Luhong Su, and Shu Chen, “Scale-free localization versus anderson localization in unidirectional quasiperiodic lattices,” *Phys. Rev. B* **111**, L140201 (2025).
- [93] Sirui Liu, Hui Jiang, Wen-Tan Xue, Qingya Li, Jiangbin Gong, Xiaogang Liu, and Ching Hua Lee, “Non-hermitian entanglement dip from scaling-induced exceptional criticality,” *Science Bulletin* **70**, 2929–2932 (2025).
- [94] Haiyu Meng, Yee Sin Ang, and Ching Hua Lee, “Generalized brillouin zone fragmentation,” arXiv preprint arXiv:2508.13275 (2025).
- [95] Xingran Xu, Lingyu Tian, Zhiyuan An, Qihua Xiong, and Sanjib Ghosh, “Exciton polariton critical non-hermitian skin effect with spin-momentum-locked gains,” *Physical Review B* **111**, L121301 (2025).
- [96] Xiaoyu Cheng, Hui Jiang, Jun Chen, Lei Zhang, Yee Sin Ang, and Ching Hua Lee, “Stochasticity-induced non-hermitian skin criticality,” arXiv preprint arXiv:2511.13176 (2025).
- [97] Zhao-Fan Cai, Tao Liu, and Zhongmin Yang, “Non-hermitian skin effect in periodically driven dissipative ultracold atoms,” *Physical Review A* **109**, 063329 (2024).
- [98] Wen-Tan Xue and Ching Hua Lee, “Topologically protected negative entanglement,” *Advanced Science* **13**, e13868 (2026).
- [99] Ruizhe Shen and Ching Hua Lee, “Non-hermitian skin clusters from strong interactions,” *Commun. Phys.* **5**, 238 (2022).
- [100] W. N. Faugno and Tomoki Ozawa, “Interaction-induced non-hermitian topological phases from a dynamical gauge field,” *Phys. Rev. Lett.* **129**, 180401 (2022).
- [101] Mingchen Zheng, Yi Qiao, Yupeng Wang, Junpeng Cao, and Shu Chen, “Exact solution of the bose-hubbard model with unidirectional hopping,” *Phys. Rev. Lett.* **132**, 086502 (2024).
- [102] Sen Mu, Ching Hua Lee, Linhu Li, and Jiangbin Gong, “Emergent fermi surface in a many-body non-hermitian fermionic chain,” *Phys. Rev. B* **102**, 081115 (2020).
- [103] Kui Cao, Qian Du, and Su-Peng Kou, “Many-body non-hermitian skin effect at finite temperatures,” *Phys. Rev. B* **108**, 165420 (2023).
- [104] Louis Garbe, Yuri Minoguchi, Julian Huber, and Peter Rabl, “The bosonic skin effect: Boundary condensation in asymmetric transport,” *SciPost Phys.* **16**, 029 (2024).
- [105] Liang Mao, Yajiang Hao, and Lei Pan, “Non-hermitian skin effect in a one-dimensional interacting bose gas,” *Phys. Rev. A* **107**, 043315 (2023).
- [106] Weixuan Zhang, Fengxiao Di, Hao Yuan, Haiteng Wang, Xingen Zheng, Lu He, Houjun Sun, and Xiangdong Zhang, “Observation of non-hermitian aggregation effects induced by strong interactions,” *Phys. Rev. B* **105**, 195131 (2022).
- [107] Ching Hua Lee, “Many-body topological and skin states without open boundaries,” *Phys. Rev. B* **104**, 195102 (2021).
- [108] Xingran Xu, Huawen Xu, S. Mandal, R. Banerjee, Sanjib Ghosh, and T. C. H. Liew, “Interaction-induced double-sided skin effect in an exciton-polariton system,” *Phys. Rev. B* **103**, 235306 (2021).
- [109] Tsuneya Yoshida, Song-Bo Zhang, Titus Neupert, and Norio Kawakami, “Non-hermitian mott skin effect,” arXiv preprint arXiv:2309.14111 (2023).
- [110] Shu Hamanaka and Kohei Kawabata, “Multifractality of many-body non-hermitian skin effect,” arXiv preprint arXiv:2401.08304 (2024).
- [111] Jacopo Gliozzi, Giuseppe De Tomasi, and Taylor L Hughes, “Many-body non-hermitian skin effect for multipoles,” *Physical review letters* **133**, 136503 (2024).
- [112] Yi Qin and Linhu Li, “Occupation-dependent particle separation in one-dimensional non-hermitian lattices,” *Phys. Rev. Lett.* **132**, 096501 (2024).
- [113] Yi Qin, Ching Hua Lee, and Linhu Li, “Dynamical suppression of many-body non-hermitian skin effect in anyonic systems,” *Communications Physics* **8**, 18 (2025).
- [114] Ruizhe Shen, Tianqi Chen, Bo Yang, and Ching Hua Lee, “Observation of the non-hermitian skin effect and fermi skin on a digital quantum computer,” *Nature Communications* **16**, 1340 (2025).
- [115] Yi Qin, Yee Sin Ang, Ching Hua Lee, and Linhu Li, “Many-body critical non-hermitian skin effect,” *Communications Physics* **9**, 16 (2026).
- [116] Martin Bonkhoff, Kevin Jägering, Shijie Hu, Axel Pelster, Sebastian Eggert, and Imke Schneider, “Anyonic phase transitions in the 1d extended hubbard model with fractional statistics,” *Phys. Rev. Lett.* **135**, 036601 (2025).
- [117] Jia-Hui Zhang, Feng Mei, Yi Li, Ching Hua Lee, Jie Ma, Liantuan Xiao, and Suotang Jia, “Observation of higher-order time-dislocation topological modes,” *Nature Communications* **16**, 2050 (2025).
- [118] Ruizhe Shen, Fang Qin, Jean-Yves Desaulles, Zlatko Papić, and Ching Hua Lee, “Enhanced many-body quantum scars from the non-hermitian fock skin effect,” *Physical Review Letters* **133**, 216601 (2024).
- [119] Jingwei Wen, Chao Zheng, Xiangyu Kong, Shijie Wei, Tao Xin, and Guilu Long, “Experimental demonstration of a digital quantum simulation of a general PT -symmetric system,” *Phys. Rev. A* **99**, 062122 (2019).
- [120] Shruti Dogra, Artem A Melnikov, and Gheorghe Sorin Paraoanu, “Quantum simulation of parity–time symmetry breaking with a superconducting quantum processor,” *Communications Physics* **4**, 26 (2021).
- [121] Feliks Kivelä, Shruti Dogra, and Gheorghe Sorin Paraoanu, “Quantum simulation of the pseudo-hermitian

Supplementary Materials

S1. ANYONIC JORDAN–WIGNER MAPPING

For completeness, we briefly review the anyonic Jordan–Wigner mapping [S1–S4] which establishes the isomorphism between 1D anyons and non-local bosons. In particular, we show that the operators \hat{a}_i , defined via the nonlocal mapping

$$\hat{a}_j = \hat{b}_j \exp\left(-i\theta \sum_{k<j} \hat{n}_k\right), \quad (\text{S1})$$

indeed satisfy the anyonic commutation relations

$$\hat{a}_i \hat{a}_j^\dagger - e^{i\theta \text{sgn}(i-j)} \hat{a}_j^\dagger \hat{a}_i = \delta_{ij}, \quad (\text{S2})$$

provided that the underlying particles \hat{b}_i obey bosonic commutation relations.

We then give a short proof. For $i < j$, we rewrite the product of anyonic operators in terms of the bosonic ones:

$$\hat{a}_i \hat{a}_j^\dagger = \hat{b}_i e^{-i\theta \sum_{i \leq k < j} \hat{n}_k} \hat{b}_j^\dagger = e^{-i\theta \sum_{i < k < j} \hat{n}_k} \hat{b}_i \hat{b}_j^\dagger e^{-i\theta \hat{n}_i}, \quad (\text{S3})$$

$$e^{i\theta \text{sgn}(i-j)} \hat{a}_j^\dagger \hat{a}_i = e^{-i\theta} e^{-i\theta \sum_{i < k < j} \hat{n}_k} e^{-i\theta \hat{n}_i} \hat{b}_j^\dagger \hat{b}_i = e^{-i\theta \sum_{i < k < j} \hat{n}_k} e^{-i\theta(\hat{n}_i+1)} \hat{b}_j^\dagger \hat{b}_i. \quad (\text{S4})$$

Subtracting the two expressions yields

$$\begin{aligned} \hat{a}_i \hat{a}_j^\dagger - e^{i\theta \text{sgn}(i-j)} \hat{a}_j^\dagger \hat{a}_i &= e^{-i\theta \sum_{i < k < j} \hat{n}_k} \left(\hat{b}_i \hat{b}_j^\dagger e^{-i\theta \hat{n}_i} - e^{-i\theta(\hat{n}_i+1)} \hat{b}_j^\dagger \hat{b}_i \right) \\ &= e^{-i\theta \sum_{i < k < j} \hat{n}_k} e^{-i\theta(\hat{n}_i+1)} [\hat{b}_i, \hat{b}_j^\dagger] = 0, \end{aligned} \quad (\text{S5})$$

which verifies the anyonic commutation relations for $i < j$.

The proof for $i > j$ follows analogously. For $i = j$, one simply notes that $\hat{a}_i^\dagger \hat{a}_i = \hat{b}_i^\dagger \hat{b}_i$ and $e^{i\theta \text{sgn}(0)} = 1$. Therefore, the mapping correctly reproduces the anyonic algebra from bosonic operators.

S2. PERTURBATION THEORY APPLIED TO DIFFERENT ENERGY CLUSTERS

To explain the unique two-stage complex plateau observed in Fig. 2 of the main text, we present a perturbative analysis in this section. The calculation indicates that the difference arises from the orders of hoppings between different subspaces, namely, a fourth-order term of $\mathcal{O}(J^2 J_p^2)$ for two particles occupying the same chain, and a second-order term of $\mathcal{O}(J_p^2)$ for them occupying different chains, as elaborated in the following subsections.

For a self-contained discussion, we begin with the anyonic Hamiltonian,

$$\begin{aligned} \hat{H} &= -J \sum_{j=1}^{L-1} \sum_{\sigma=A,B} \left(e^{\alpha\sigma} \hat{a}_{j,\sigma}^\dagger \hat{a}_{j+1,\sigma} + e^{-\alpha\sigma} \hat{a}_{j+1,\sigma}^\dagger \hat{a}_{j,\sigma} \right) \\ &+ J_p \sum_{j=1}^L \left(\hat{a}_{j,A}^\dagger \hat{a}_{j,B} + \hat{a}_{j,B}^\dagger \hat{a}_{j,A} \right) + \mu \sum_{j=1}^L (\hat{n}_{j,A} - \hat{n}_{j,B}) \\ &+ \frac{U}{2} \sum_{j=1}^L \sum_{\sigma=A,B} \hat{n}_{j,\sigma} (\hat{n}_{j,\sigma} - 1). \end{aligned} \quad (\text{S6})$$

The anyonic creation/annihilation operators satisfy

$$\begin{aligned} [\hat{a}_j, \hat{a}_k]_\theta &\equiv \hat{a}_j \hat{a}_k - e^{-i\theta \text{sgn}(j-k)} \hat{a}_k \hat{a}_j = 0, \\ [\hat{a}_j, \hat{a}_k^\dagger]_{-\theta} &\equiv \hat{a}_j \hat{a}_k^\dagger - e^{i\theta \text{sgn}(j-k)} \hat{a}_k^\dagger \hat{a}_j = \delta_{jk}, \end{aligned} \quad (\text{S7})$$

We rewrite the Hamiltonian as $\hat{H} = \hat{H}_0 + \hat{V}$,

$$\hat{H}_0 = \hat{H}_\mu + \hat{H}_U, \quad \hat{V} = \hat{H}_J + \hat{H}_{J_p}, \quad (\text{S8})$$

with $\hat{H}_\mu = \mu \sum_j (\hat{n}_{j,A} - \hat{n}_{j,B})$ and $\hat{H}_U = \frac{U}{2} \sum_{j,\sigma} \hat{n}_{j,\sigma} (\hat{n}_{j,\sigma} - 1)$. \hat{H}_J and \hat{H}_{J_p} denote the intra-chain and inter-chain hopping terms, respectively.

In the two-particle sector, a convenient (unnormalized) basis is

$$|j, \sigma; k, \sigma'\rangle \equiv \hat{a}_{j,\sigma}^\dagger \hat{a}_{k,\sigma'}^\dagger |0\rangle, \quad (\text{S9})$$

with $j = k$ and $\sigma' = \sigma$ for on-site doublons.

A. Strong-coupling perturbation theory in the lowest BB scattering subspace (two particles)

The key result of this subsection is that the anyonic statistical phase enters the plaquette-assisted exchange only at fourth order, as captured by Eq. (S24).

For scattering states ($j \neq k$) the interaction part does not contribute, hence

$$\hat{H}_0 |j, \sigma; k, \sigma'\rangle = E_{\sigma\sigma'}^{(0)} |j, \sigma; k, \sigma'\rangle, \quad E_{\sigma\sigma'}^{(0)} = (s_\sigma + s_{\sigma'})\mu, \quad s_A = +1, \quad s_B = -1. \quad (\text{S10})$$

Thus

$$E_{AA}^{(0)} = +2\mu, \quad E_{AB}^{(0)} = 0, \quad E_{BB}^{(0)} = -2\mu. \quad (\text{S11})$$

Assuming $\mu > 0$, the lowest scattering manifold is the BB sector. Define the projector onto the *lowest BB scattering subspace*

$$P \equiv \sum_{1 \leq j \neq k \leq L} |j, B; k, B\rangle \langle j, B; k, B|, \quad Q \equiv 1 - P. \quad (\text{S12})$$

We denote the unperturbed energy in this manifold by $E_0 = -2\mu$.

The interchain term \hat{H}_{J_p} flips the chain index on a single site:

$$\hat{H}_{J_p} : \quad B \leftrightarrow A. \quad (\text{S13})$$

Therefore, any process that starts in the BB subspace and ends in the BB subspace must contain an *even* number of \hat{H}_{J_p} insertions. In particular, all odd-order contributions containing an odd power of J_p vanish after projection back to P :

$$P(\dots \hat{H}_{J_p} \dots)P = 0 \quad \text{if the total number of } \hat{H}_{J_p} \text{ is odd.} \quad (\text{S14})$$

This immediately implies that all odd-order hopping processes vanish; therefore, we only need to consider even orders.

Using (degenerate) Schrieffer–Wolff / Brillouin–Wigner expansion [S5, S6], the projected effective Hamiltonian reads

$$\hat{H}_{\text{eff}} = P\hat{H}_0P + P\hat{V}P - P\hat{V}Q \frac{1}{\hat{H}_0 - E_0} Q\hat{V}P + P\hat{V}Q \frac{1}{\hat{H}_0 - E_0} Q\hat{V}Q \frac{1}{\hat{H}_0 - E_0} Q\hat{V}P + \dots \quad (\text{S15})$$

Within P , $P\hat{H}_0P = E_0P$ is a constant shift.

Since \hat{H}_{J_p} exchanges the chain indexes, $P\hat{H}_{J_p}P = 0$. Hence

$$\hat{H}_{\text{eff}}^{(1)} = P\hat{H}_{J_p}P, \quad (\text{S16})$$

which generates the kinetic motion of two particles on the B chain (with non-reciprocal hopping $e^{\pm\alpha_B}$). No exchange phase θ appears at this order. All third-order contributions either vanish by the chain-parity selection rule (an odd number of H_{J_p} cannot return to the BB manifold), or contain at most one spatial hop and thus cannot realize a two-particle exchange loop; consequently no θ -dependent term can appear at third order. The leading exchange process requires two H_{J_p} insertions and two spatial hoppings, i.e., it first arises at $\mathcal{O}(J^2 J_p^2)$.

At second order, only the two-channel loops J^2 and J_p^2 survive:

$$\hat{H}_{\text{eff}}^{(2)} = -P\hat{H}_JQ \frac{1}{\hat{H}_0 - E_0} Q\hat{H}_JP - P\hat{H}_{J_p}Q \frac{1}{\hat{H}_0 - E_0} Q\hat{H}_{J_p}P. \quad (\text{S17})$$

- The J^2 term proceeds via a BB doublon intermediate state, e.g. $|j, B; j+1, B\rangle \rightarrow |j, B; j, B\rangle \rightarrow |j, B; j+1, B\rangle$, with energy denominator

$$\Delta_U = (U - 2\mu) - (-2\mu) = U. \quad (\text{S18})$$

It produces an energy correction only when the two particles become adjacent (a nearest-neighbor projector in the two-particle subspace), but does not involve particle exchange and hence does not generate θ .

- The J_p^2 term proceeds via an AB scattering intermediate state, $|BB\rangle \rightarrow |AB\rangle \rightarrow |BB\rangle$, with denominator

$$\Delta_\mu = 0 - (-2\mu) = 2\mu, \quad (\text{S19})$$

leading to a uniform shift within the BB scattering manifold (no exchange structure, no θ). Therefore, All second-order contributions within P are independent of θ .

We next provide an explicit fourth-order virtual process that generates the anyonic exchange phase without ever visiting an intrachain doublon (hence without any U -denominators). For clarity we work in an oriented two-particle basis $|j, \sigma; k, \sigma'\rangle \equiv \hat{a}_{j,\sigma}^\dagger \hat{a}_{k,\sigma'}^\dagger |0\rangle$ with $j \neq k$, so that $|k, \sigma'; j, \sigma\rangle = e^{+i\theta \text{sgn}(k-j)} |j, \sigma; k, \sigma'\rangle$. We evaluate the fourth-order matrix element connecting the two ordered nearest-neighbor BB states $|i\rangle \equiv |j, B; j+1, B\rangle$ and $|f\rangle \equiv |j+1, B; j, B\rangle$ within the projected strong-coupling expansion

$$\hat{H}_{\text{eff}}^{(4)} = P \hat{V} \frac{1}{E_0 - \hat{H}_0} Q \hat{V} \frac{1}{E_0 - \hat{H}_0} Q \hat{V} \frac{1}{E_0 - \hat{H}_0} Q \hat{V} P, \quad (\text{S20})$$

with $E_0 = -2\mu$ and $\hat{V} = \hat{H}_J + \hat{H}_{J_p}$.

Starting from $|i\rangle$, the minimal ‘‘plaquette’’ sequence on the ladder is

$$(j, B; j+1, B) \xrightarrow{J_p \text{ at } j} (j, A; j+1, B) \xrightarrow{J \text{ on } B} (j, A; j, B) \xrightarrow{J \text{ on } A} (j+1, A; j, B) \xrightarrow{J_p \text{ at } j+1} (j+1, B; j, B) = |f\rangle.$$

Denoting the intermediate states by $|m_1\rangle \equiv |j, A; j+1, B\rangle$, $|m_2\rangle \equiv \hat{a}_{j,B}^\dagger \hat{a}_{j,A}^\dagger |0\rangle$, and $|m_3\rangle \equiv |j+1, A; j, B\rangle$, their unperturbed energies under $\hat{H}_0 = \hat{H}_\mu + \hat{H}_U$ are all $E_{m_1} = E_{m_2} = E_{m_3} = 0$ (they belong to the AB sector and carry no intrachain doublon penalty), while $E_0 = -2\mu$ in the BB manifold. Hence each energy denominator equals

$$E_0 - E_{m_\ell} = -2\mu, \quad \ell = 1, 2, 3. \quad (\text{S21})$$

The corresponding vertex matrix elements are

$$\langle m_1 | \hat{H}_{J_p} | i \rangle = J_p, \quad \langle f | \hat{H}_{J_p} | m_3 \rangle = J_p, \quad (\text{S22})$$

$$\langle m_3 | \hat{H}_J | m_2 \rangle = -J e^{-\alpha_A}, \quad \langle m_2 | \hat{H}_J | m_1 \rangle = -J e^{\alpha_B} e^{+i\theta}. \quad (\text{S23})$$

The anyonic phase arises solely from commuting $\hat{a}_{j+1,B}$ through $\hat{a}_{j,A}^\dagger$ when acting with the B -chain hop $\hat{a}_{j,B}^\dagger \hat{a}_{j+1,B}$ on $|m_1\rangle$, i.e., $\hat{a}_{j+1,B} \hat{a}_{j,A}^\dagger = e^{+i\theta} \hat{a}_{j,A}^\dagger \hat{a}_{j+1,B}$. Collecting all factors, this single virtual path contributes to the exchange matrix element

$$\langle f | \hat{H}_{\text{eff}}^{(4)} | i \rangle \supset \frac{\langle f | \hat{H}_{J_p} | m_3 \rangle \langle m_3 | \hat{H}_J | m_2 \rangle \langle m_2 | \hat{H}_J | m_1 \rangle \langle m_1 | \hat{H}_{J_p} | i \rangle}{(E_0 - E_{m_1})(E_0 - E_{m_2})(E_0 - E_{m_3})} = -\frac{J^2 J_p^2}{8\mu^3} e^{(\alpha_B - \alpha_A)} e^{+i\theta}. \quad (\text{S24})$$

The time-reversed plaquette sequence produces the complex-conjugate anyonic factor $e^{-i\theta}$ and the reciprocal non-Hermiticity factor $e^{-(\alpha_B - \alpha_A)}$, leading at $\mathcal{O}(J^2 J_p^2)$ to the effective two-body exchange operator that couples the two ordered nearest-neighbor BB configurations with amplitudes proportional to $e^{\pm i\theta}$.

The expansion is controlled when the virtual gaps associated with leaving P are large compared with the perturbations:

$$U \gg J, \quad 2\mu \gg J_p, \quad (\text{S25})$$

and $\mu > 0$ to ensure the BB scattering manifold is the lowest-energy scattering sector.

In summary, with $H_0 = H_\mu + H_U$ and projection to the lowest BB scattering subspace, (i) all contributions up to second order are independent of θ ; (ii) anyonic statistics enters the effective theory first through a fourth-order exchange term of order $J^2 J_p^2$. All virtual processes that connect $|j, B; k, B\rangle$ and $|k, B; j, B\rangle$ within the lowest BB scattering manifold must involve an even number of interchain couplings and at least two spatial hoppings. Consequently, all exchange processes first appear at fourth order $\mathcal{O}(J^2 J_p^2)$ and reduce to the same effective two-body exchange operator, differing only in their numerical prefactors. No additional independent exchange terms exist at the same or lower order.

B. Second-order perturbation theory in the AB two-particle sector

The key result of this subsection is that the earliest effective signature of anyonic statistics already appears in the AB two-particle sector through the second-order exchange amplitude in Eq. S36.

We consider the two-particle Hilbert space with one particle on chain A and the other on chain B ,

$$\mathcal{H}_{AB} = \text{span}\{|j, k\rangle_{AB} = \hat{a}_{j,A}^\dagger \hat{a}_{k,B}^\dagger |0\rangle \mid j \neq k\}. \quad (\text{S26})$$

Throughout, we adopt the real-space embedding

$$A : 1, \dots, L, \quad B : L + 1, \dots, 2L, \quad (\text{S27})$$

so that any reordering between A - and B -chain operators carries an anyonic phase.

The unperturbed Hamiltonian is chosen as $\hat{H}_0 = \hat{H}_\mu + \hat{H}_U$ as defined in eq. S8. For states $|j, k\rangle_{AB}$ with $j \neq k$, there is no on-site interaction, and the chemical potential contributions cancel,

$$E_{AB}^{(0)} = 0. \quad (\text{S28})$$

The relevant intermediate states generated by inter-chain tunneling are

$$E_{AA}^{(0)} = +2\mu, \quad (\text{S29})$$

$$E_{BB}^{(0)} = -2\mu. \quad (\text{S30})$$

We focus on the inter-chain hopping

$$V \equiv H_{J_p} = J_p \sum_{\ell} \left(\hat{a}_{\ell,A}^\dagger \hat{a}_{\ell,B} + \hat{a}_{\ell,B}^\dagger \hat{a}_{\ell,A} \right) \quad (\text{S31})$$

and treat it as a perturbation (the intra-chain hopping H_J can be omitted since in the AB two-particle scattering sector, it alone does not produce a net θ -dependence because it cannot generate an exchange process that changes the particle ordering.) The second-order effective Hamiltonian within \mathcal{H}_{AB} is given by

$$\langle f | H_{\text{eff}}^{(2)} | i \rangle = \sum_{m \notin \mathcal{H}_{AB}} \frac{\langle f | V | m \rangle \langle m | V | i \rangle}{E_{AB}^{(0)} - E_m^{(0)}}. \quad (\text{S32})$$

We focus on the exchange matrix element between

$$|i\rangle = |j, k\rangle_{AB}, \quad |f\rangle = |k, j\rangle_{AB}, \quad j \neq k. \quad (\text{S33})$$

There are two virtual processes contributing at second order:

1. a path via the BB intermediate state,
2. a path via the AA intermediate state.

Because of the anyonic commutation relations and the real-space embedding, operator reordering between A and B chains generates statistical phase factors. A direct evaluation shows that the BB path contributes

$$\langle k, j | H_{\text{eff}}^{(2)} | j, k \rangle_{BB} = \frac{J_p^2}{2\mu} e^{-i\theta \text{sgn}(j-k)}, \quad (\text{S34})$$

while the AA path contributes

$$\langle k, j | H_{\text{eff}}^{(2)} | j, k \rangle_{AA} = -\frac{J_p^2}{2\mu} e^{i\theta \text{sgn}(j-k)}. \quad (\text{S35})$$

Summing the two contributions, we obtain the total second-order exchange matrix element

$$\langle k, j | H_{\text{eff}}^{(2)} | j, k \rangle = \frac{J_p^2}{2\mu} \left[e^{-i\theta \text{sgn}(j-k)} - e^{i\theta \text{sgn}(j-k)} \right]. \quad (\text{S36})$$

Several important conclusions follow immediately:

- For $\theta = 0$, the contributions from the AA and BB virtual paths cancel exactly, and the second-order exchange matrix element vanishes.
- For $\theta \neq 0$ and $j \neq k$, a finite exchange coupling is generated already at second order.
- The statistical phase originates from operator reordering between A - and B -chain particles under the real-space embedding, rather than from spatial hopping.

Thus, when the two particles initially occupy different sites on different chains, inter-chain tunneling induces an effective anyonic exchange at second order, which fundamentally distinguishes the cases $\theta = 0$ and $\theta \neq 0$. Including intra-chain hopping introduces a first-order contribution to the non-Hermitian hopping. Together with the statistical-angle effect, this makes the energy spectrum complex.

S3. PSEUDO-HERMITICITY BREAKING IN THE ANYONIC LADDER MODEL

We consider the two-chain bosonic Hamiltonian derived from anyonic model using the above transformation,

$$\begin{aligned} \hat{H} = & - \sum_{j=1}^{L-1} \sum_{\sigma=A,B} \left(J_{L,\sigma} \hat{b}_{j,\sigma}^\dagger e^{-i\theta \hat{n}_{j,\sigma}} \hat{b}_{j+1,\sigma} + J_{R,\sigma} \hat{b}_{j+1,\sigma}^\dagger e^{i\theta \hat{n}_{j,\sigma}} \hat{b}_{j,\sigma} \right) \\ & + \sum_{j=1}^L \left(J_p e^{i\theta \Phi_j} \hat{b}_{j,B}^\dagger \hat{b}_{j,A} + J_p \hat{b}_{j,A}^\dagger \hat{b}_{j,B} e^{-i\theta \Phi_j} \right) + \frac{U}{2} \sum_{j=1,\sigma}^L \hat{n}_{j,\sigma} (\hat{n}_{j,\sigma} - 1) + \mu \sum_{j=1}^L (\hat{n}_{j,A} - \hat{n}_{j,B}), \end{aligned} \quad (\text{S37})$$

where

$$\Phi_j = \sum_{k=j}^L \hat{n}_{k,A} + \sum_{k=1}^{j-1} \hat{n}_{k,B}, \quad J_{L,\sigma} = J e^{\alpha_\sigma}, \quad J_{R,\sigma} = J e^{-\alpha_\sigma}, \quad \alpha_A = \alpha, \quad \alpha_B = -\alpha.$$

We now define the pseudo-Hermiticity operator as:

$$\mathcal{K} := \mathcal{R}_z \mathcal{I} \mathcal{T},$$

where \mathcal{T} is time-reversal (complex conjugation), \mathcal{I} is the spatial inversion operator: $j \rightarrow L+1-j$, acts identically on both chains, $\mathcal{R}_z = \exp\left(-i\theta \sum_{j=1}^L \sum_{\sigma=A,B} \frac{\hat{n}_{j,\sigma}(\hat{n}_{j,\sigma}-1)}{2}\right)$ is a local density-dependent rotation. Action of \mathcal{K} on field operators:

$$\mathcal{I} \hat{b}_{j,\sigma} \mathcal{I}^\dagger = \hat{b}_{L+1-j,\sigma}, \quad \mathcal{R}_z \hat{b}_{j,\sigma} \mathcal{R}_z^\dagger = e^{i\theta \hat{n}_{j,\sigma}} \hat{b}_{j,\sigma}, \quad \mathcal{R}_z \hat{b}_{j,\sigma}^\dagger \mathcal{R}_z^\dagger = \hat{b}_{j,\sigma}^\dagger e^{-i\theta \hat{n}_{j,\sigma}}.$$

Thus, for the total \mathcal{K} , we obtain:

$$\mathcal{K} \hat{b}_{j,\sigma} \mathcal{K}^\dagger = e^{i\theta \hat{n}_{L+1-j,\sigma}} \hat{b}_{L+1-j,\sigma}, \quad \mathcal{K} \hat{b}_{j,\sigma}^\dagger \mathcal{K}^\dagger = \hat{b}_{L+1-j,\sigma}^\dagger e^{-i\theta \hat{n}_{L+1-j,\sigma}}.$$

Each chain's Hamiltonian

$$\hat{H}_\sigma = - \sum_{j=1}^{L-1} \left(J_{L,\sigma} \hat{b}_{j,\sigma}^\dagger e^{-i\theta \hat{n}_{j,\sigma}} \hat{b}_{j+1,\sigma} + J_{R,\sigma} \hat{b}_{j+1,\sigma}^\dagger e^{i\theta \hat{n}_{j,\sigma}} \hat{b}_{j,\sigma} \right) + \frac{U}{2} \sum_j \hat{n}_{j,\sigma} (\hat{n}_{j,\sigma} - 1)$$

satisfies:

$$\mathcal{K} \hat{H}_\sigma \mathcal{K}^\dagger = \hat{H}_\sigma^\dagger,$$

i.e., each single chain is pseudo-Hermitian under \mathcal{K} .

For inter-chain coupling term, we examine:

$$\hat{H}_{AB} = J_p \sum_{j=1}^L \left(e^{i\theta \Phi_j} \hat{b}_{j,B}^\dagger \hat{b}_{j,A} + \text{h.c.} \right), \quad \Phi_j = \sum_{k=j}^L \hat{n}_{k,A} + \sum_{k=1}^{j-1} \hat{n}_{k,B}.$$

Under $\mathcal{K} = \mathcal{R}_z \mathcal{IT}$, one finds:

$$\mathcal{K} \left(\hat{b}_{j,B}^\dagger \hat{b}_{j,A} \right) \mathcal{K}^\dagger = \hat{b}_{L+1-j,B}^\dagger e^{-i\theta \hat{n}_{L+1-j,B}} \cdot e^{i\theta \hat{n}_{L+1-j,A}} \hat{b}_{L+1-j,A},$$

which gives:

$$\mathcal{K} \left(\hat{b}_{j,B}^\dagger \hat{b}_{j,A} \right) \mathcal{K}^\dagger = \hat{b}_{L+1-j,B}^\dagger \hat{b}_{L+1-j,A} \cdot e^{i\theta(\hat{n}_{L+1-j,A} - \hat{n}_{L+1-j,B})}.$$

However, the Peierls phase transforms as:

$$\Phi_j \rightarrow \Phi'_j = \sum_{k=L+1-j}^L \hat{n}_{k,A} + \sum_{k=1}^{L-j} \hat{n}_{k,B}.$$

Hence:

$$\mathcal{K} \hat{H}_{AB} \mathcal{K}^\dagger \neq \hat{H}_{AB}^\dagger.$$

From the above calculations, we note that although each chain individually respects pseudo-Hermiticity under $\mathcal{K} = \mathcal{R}_z \mathcal{IT}$, the full two-chain Hamiltonian fails to satisfy it,

$$\mathcal{K} \hat{H} \mathcal{K}^\dagger \neq \hat{H}^\dagger,$$

because the nonlocal Peierls phase Φ_j breaks inversion symmetry \mathcal{I} while keeping the others.

Explicitly, the inter-chain couplings in the double-chain bosonic Hamiltonian reads

$$\hat{H}_{AB} = J_p \sum_{j=1}^L \left(e^{i\theta \Phi_j} \hat{b}_{j,B}^\dagger \hat{b}_{j,A} + \text{h.c.} \right), \quad \Phi_j = \sum_{k=j}^L \hat{n}_{k,A} + \sum_{k=1}^{j-1} \hat{n}_{k,B},$$

and the symmetry operation yields

$$\begin{aligned} \mathcal{K} \left(e^{i\theta \Phi_j} \hat{b}_{j,B}^\dagger \hat{b}_{j,A} \right) \mathcal{K}^\dagger &= \mathcal{R}_z \cdot \mathcal{I} \cdot \mathcal{T} \left(e^{i\theta \Phi_j} \hat{b}_{j,B}^\dagger \hat{b}_{j,A} \right) \mathcal{T}^{-1} \cdot \mathcal{I}^{-1} \cdot \mathcal{R}_z^\dagger \\ &= e^{-i\theta \Phi'_j} \cdot \mathcal{R}_z \left(\hat{b}_{L+1-j,B}^\dagger \hat{b}_{L+1-j,A} \right) \mathcal{R}_z^\dagger \\ &= e^{-i\theta \Phi'_j} \cdot \hat{b}_{L+1-j,B}^\dagger e^{i\theta(\hat{n}_{L+1-j,A} - \hat{n}_{L+1-j,B})} \hat{b}_{L+1-j,A}, \end{aligned}$$

with

$$\Phi'_j = \sum_{k=L+1-j}^L \hat{n}_{k,A} + \sum_{k=1}^{L-j} \hat{n}_{k,B}.$$

In contrast to the original term, the transformed expression includes an additional operator-valued phase factor $e^{i\theta(\hat{n}_A - \hat{n}_B)}$ and the number-dependent Φ'_j does not map back to any Φ_j in the original form. As a result,

$$\mathcal{K} \hat{H}_{AB} \mathcal{K}^\dagger \neq \hat{H}_{AB}^\dagger.$$

Thus, inter-chain coupling invalidates pseudo-Hermiticity of the total system for anyons, leading to complex eigenenergies not necessarily forming conjugate pairs. This is the novelty of our model in the main text.

S4. EVOLUTION OF EIGENENERGIES WITH THE INCREASE OF COUPLING STRENGTHS

As discussed in the main text, we emphasize that the jump of the maximal imaginary energy is tied to a *two-fold degeneracy* of the maximal $\text{Im } E$ for anyons. To give a clear view, we plot the imaginary energy levels versus J_p for two anyonic cases in Fig. S1. As can be seen in the zoom in view near the crossing of $\max \text{Im } E$, the maximal imaginary energy becomes nearly two-fold degenerate (with a small finite-size spacing in between) there after, which leads to the strong oscillation of the long-time quench dynamics in Fig. 4(a) of the main text.

It should be noted that the pseudo-Hermitian symmetry-breaking behavior for $\theta = 0$ and π is quantitatively different from that for $\theta = 0.4\pi$ and 0.8π , as shown in Fig. S2 for $N = 3$. Specifically, for sufficiently small (large) coupling, the spectrum remains real (complex) for all values of θ . The key difference is that the number of growing and decaying states is significantly larger for θ away from $\theta = 0$ and $\theta = \pi$.

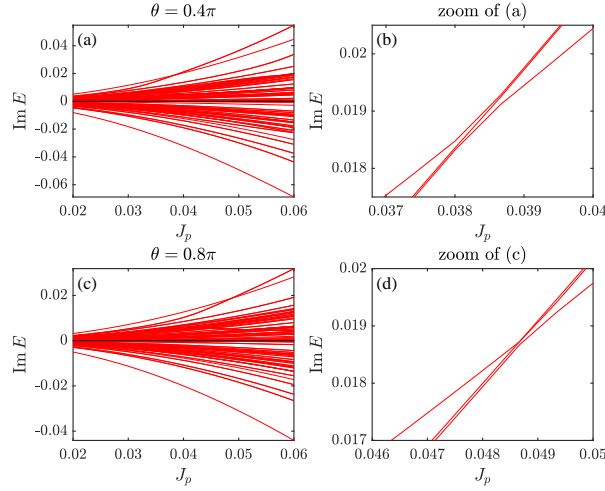


FIG. S1. (a) Imaginary energy levels around the crossing point for $\theta = 0.4\pi$. (b) The same as (a) zoom in around the crossing point. (c), (d) the same as that of (a), (b) but for $\theta = 0.8\pi$. We observe two states are nearly degenerate. Parameters are $U = 16, \mu = 4, L = 10, J_e^\alpha = 0.5, J_e^{-\alpha} = 1$.

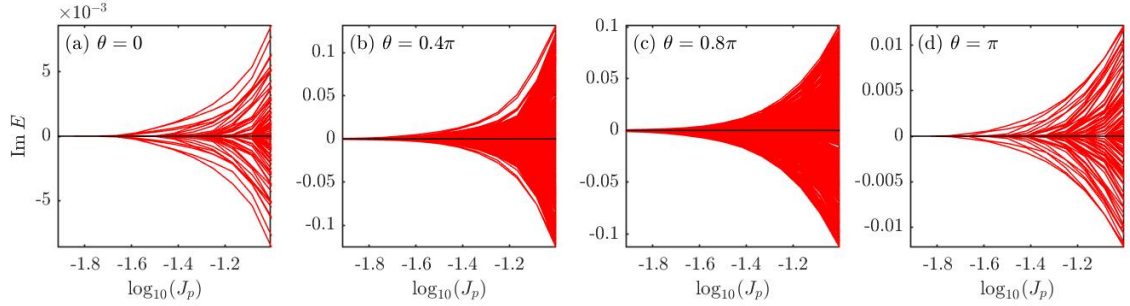


FIG. S2. Imaginary energy spectrum for $N = 3$, illustrating the effect of AIST. The results reveal the statistical angle as a powerful control knob for the non-Hermitian spectrum. While the differences between $\theta = 0.4\pi, 0.8\pi$ and $\theta = 0, \pi$ are mainly quantitative, varying the statistical angle markedly reshapes the spectral distribution. In particular, the anyonic cases exhibit a lower critical coupling for the onset of complex eigenvalues, together with a broader and more densely populated distribution of imaginary parts than the non-anyonic cases $\theta = 0, \pi$. Other parameters are the same as Fig. S1.

S5. QUENCH FROM THE BAND WITH MAXIMUM IMAGINARY EIGENVALUES

A. More understanding of the stability by decomposing the dynamics

In order to understand the stability of anyons and the oscillations of bosons for $t < 2000$, we evaluate the population on each eigenstate of the post-quench Hamiltonian. A simple calculation yields

$$\begin{aligned}
 |\psi(t)\rangle &= e^{-iHt}|\psi(0)\rangle \\
 &= \sum_n e^{-iHt}|\psi_n^R\rangle\langle\psi_n^L|\psi(0)\rangle \\
 &= \sum_n e^{-iE_n t}|\psi_n^R\rangle\langle\psi_n^L|\psi(0)\rangle \\
 &= \sum_n e^{-iE_n t}\langle\psi_n^L|\psi(0)\rangle|\psi_n^R\rangle \\
 &= \sum_n c_n(t)|\psi_n^R\rangle,
 \end{aligned} \tag{S38}$$

where

$$c_n(t) = e^{-iE_n t} \langle \psi_n^L | \psi(0) \rangle = \langle \psi_n^L | \psi(t) \rangle. \quad (\text{S39})$$

The superscript L and R denote the left and right eigenstates of Hamiltonian H , respectively.

For bosons and pseudofermions, several eigenstates contribute within the time window 0-2000, as shown in Fig. S3. Since these eigenstates either decay or grow during the evolution, oscillations appear in the function $P(t)$. In contrast, for anyons with $\theta = 0.4\pi$ and 0.8π , only a single eigenstate contributes within the same time window, which accounts for their stability. However, beyond $t \approx 2000$, bosons and pseudofermions are dominated by a single state with the largest imaginary component, while for anyons two nearly degenerate eigenstates emerge, leading to strong oscillations.

To intuitively understand the transition of $P(t)$, we use a two-state approximation. Suppose at the initial stage of the dynamics, the state can be approximated by the two leading eigenstates of the post-quench Hamiltonian,

$$|\psi(t)\rangle \approx c_1 e^{-iE_1 t} |\psi_{E_1}\rangle + c_2 e^{-iE_2 t} |\psi_{E_2}\rangle. \quad (\text{S40})$$

The initial state has a larger overlap with $|\psi_{E_1}\rangle$, corresponding to the smaller Im, E , and the dynamics will evolve toward $|\psi_{E_2}\rangle$ provided that $\text{Im}, E_2 > \text{Im}, E_1$. The corresponding time-dependent coefficients are

$$c_1(t) = c_1 e^{-iE_1 t}, \quad c_2(t) = c_2 e^{-iE_2 t}. \quad (\text{S41})$$

The ratio of their amplitudes evolves as

$$\frac{|c_1(t)|}{|c_2(t)|} = \frac{c_1}{c_2} e^{(\text{Im}E_1 - \text{Im}E_2)t}. \quad (\text{S42})$$

Assuming $c_1/c_2 \approx 10^{-7}$ and $\text{Im}E_2 - \text{Im}E_1 = 0.008$, the crossover time is estimated as

$$t = \frac{\ln(c_1/c_2)}{\text{Im}E_2 - \text{Im}E_1} \sim 10^3. \quad (\text{S43})$$

To quantify how many eigenstates participate in the evolution, we define the inverse participation ratio (IPR) in the Fock basis,

$$\text{IPR} = \sum_n |\langle n | \psi(t) \rangle|^4. \quad (\text{S44})$$

As shown in Fig. S4, the low IPR values and their oscillatory behavior indicate that more Fock states are involved and vary during the evolution.

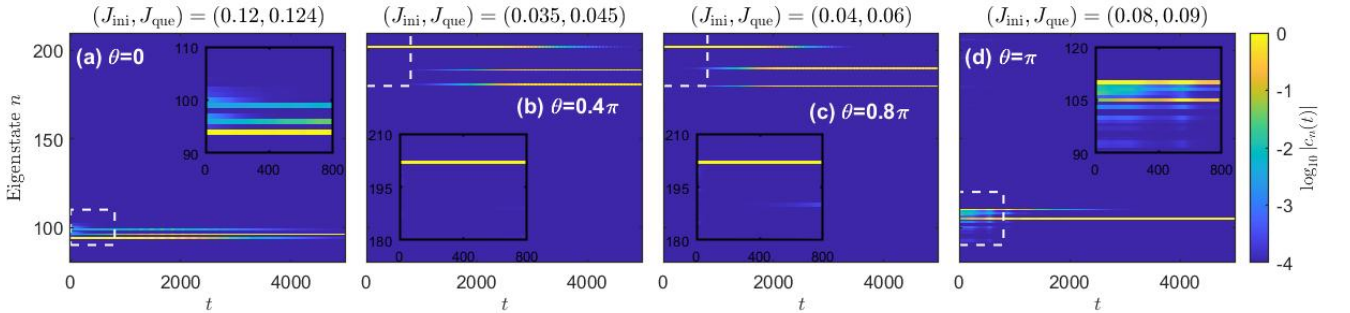


FIG. S3. Decomposition into the eigenstates of the post-quench Hamiltonian for different values of θ . Insets show zoomed-in views of the corresponding panels. Parameters: $L = 10, N = 2, U = 16, \mu = 4$.

B. Density of states of imaginary energy for the post quench Hamiltonian

In this subsection, we present the density of states (DOS) of the imaginary eigenvalues of the post-quench Hamiltonian, as shown in Fig. S5. The energy spectrum is asymmetric with respect to $\text{Im}E = 0$, which arises from the breaking of pseudo-Hermitian symmetry. For bosons and pseudofermions, the imaginary part of the energy remains very close to zero.

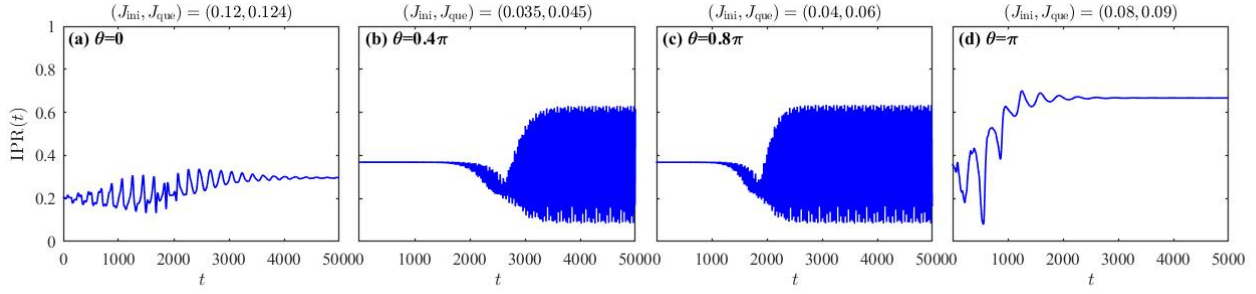


FIG. S4. IPR by decomposing $|\psi(t)\rangle$ into Fock basis for different values of θ . $L = 10, N = 2, U = 16, \mu = 4$.

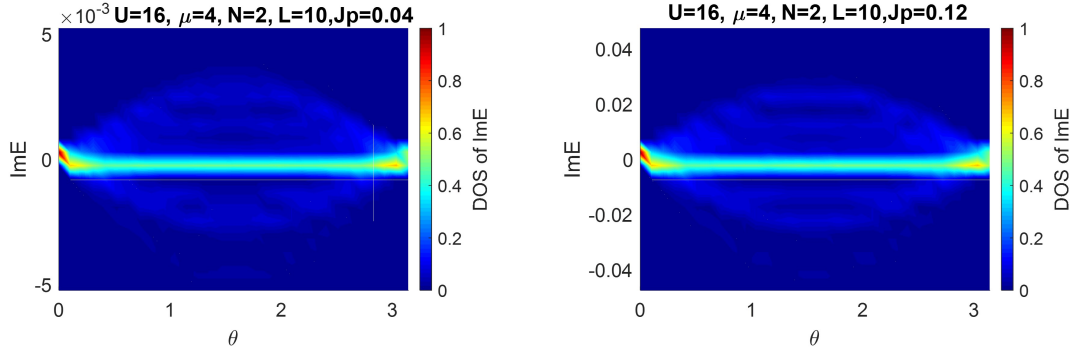


FIG. S5. Density of states (DOS) of imaginary energy of the post quench Hamiltonian for two different coupling strengths. $L = 10, N = 2, U = 16, \mu = 4$.

S6. TESTING THE NOVEL DYNAMICAL STABILITY UNDER DIFFERENT PARAMETERS

A. Test for the stability for different quench parameters

In this subsection, we calculate additional data for different quench values of $J_{\text{ini}} = J_i$ and $J_{\text{que}} = J_f$. The results are shown in Fig. S6, which indicate that, under the same quench protocol, the dynamics of anyons is consistently more stable than that of bosons and pseudofermions.

B. Test for the stability of other θ

First, we calculate the edge correlation function for different statistical angles θ , and the results are shown in Fig. S7. The results indicate that the boundary correlation is sensitive to all values of θ .

Then, we quench the system from a smaller J_p (J_{ini}) to a larger J_p (J_{que}), as in the main text. The results are shown in Fig. S8. These results indicate that the quench dynamics remains stable at short times, regardless of the choice of quench parameters.

-
- [S1] F. Liu, J. R. Garrison, D.-L. Deng, Z.-X. Gong, and A. V. Gorshkov, *Phys. Rev. Lett.* **121**, 250404 (2018).
[S2] F. Lange, S. Ejima, and H. Fehske, *Phys. Rev. Lett.* **118**, 120401 (2017).
[S3] Y. Qin, C. H. Lee, and L. Li, *Communications Physics* **8**, 18 (2025).
[S4] M. Bonkhoff, K. Jägering, S. Hu, A. Pelster, S. Eggert, and I. Schneider, *Phys. Rev. Lett.* **135**, 036601 (2025).
[S5] D. C. Zheng, B. R. Barrett, J. P. Vary, and R. J. McCarthy, *Phys. Rev. C* **49**, 1999 (1994).
[S6] T. J. Fields, K. S. Gupta, and J. P. Vary, *Modern Physics Letters A* **11**, 2233 (1996), arXiv:hep-ph/9506320 [hep-ph].

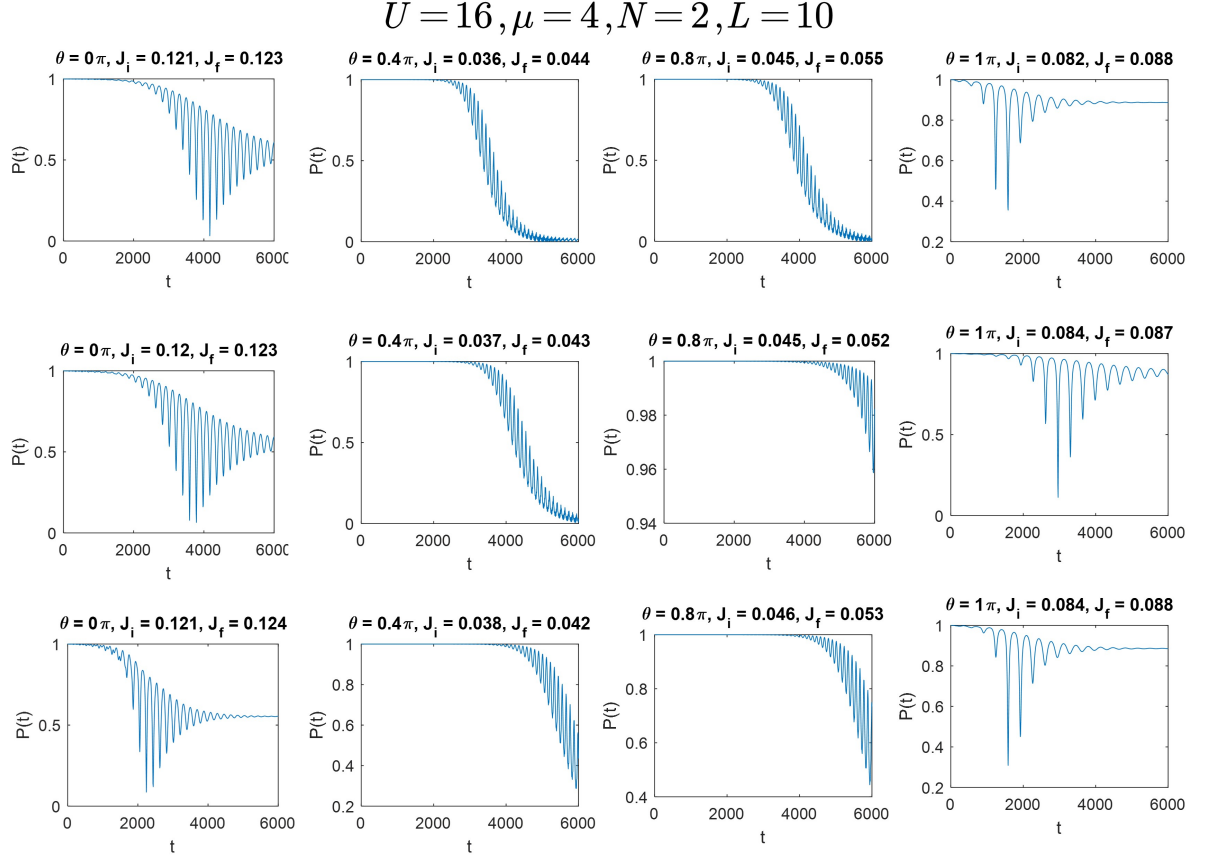


FIG. S6. Different pairs of $J_{\text{ini}} = J_i$ and $J_{\text{que}} = J_f$ for various θ . Parameters: $L = 10, N = 2, U = 16, \mu = 4$.

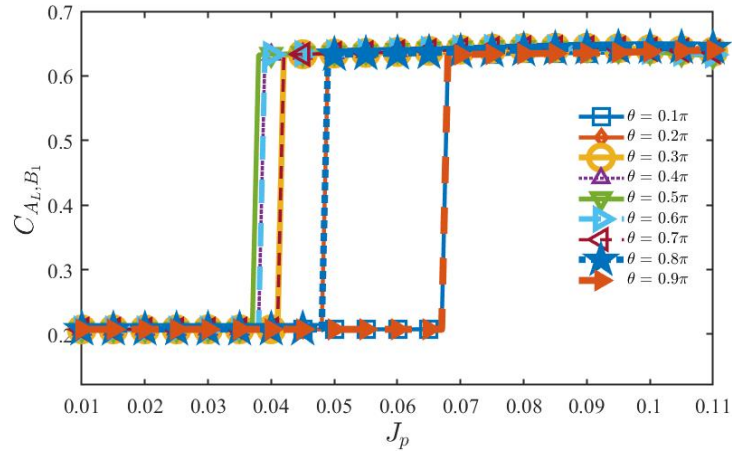


FIG. S7. The jump in the edge correlation function. Edge correlation function $C_{A_L, B_1} = \langle \psi | \hat{n}_{A, L} \hat{n}_{B, 1} | \psi \rangle$. $|\psi\rangle$ is the eigenstate with maximum imaginary energy for a specific J_p . Parameters: $L = 10, N = 2, U = 16, \mu = 4$.

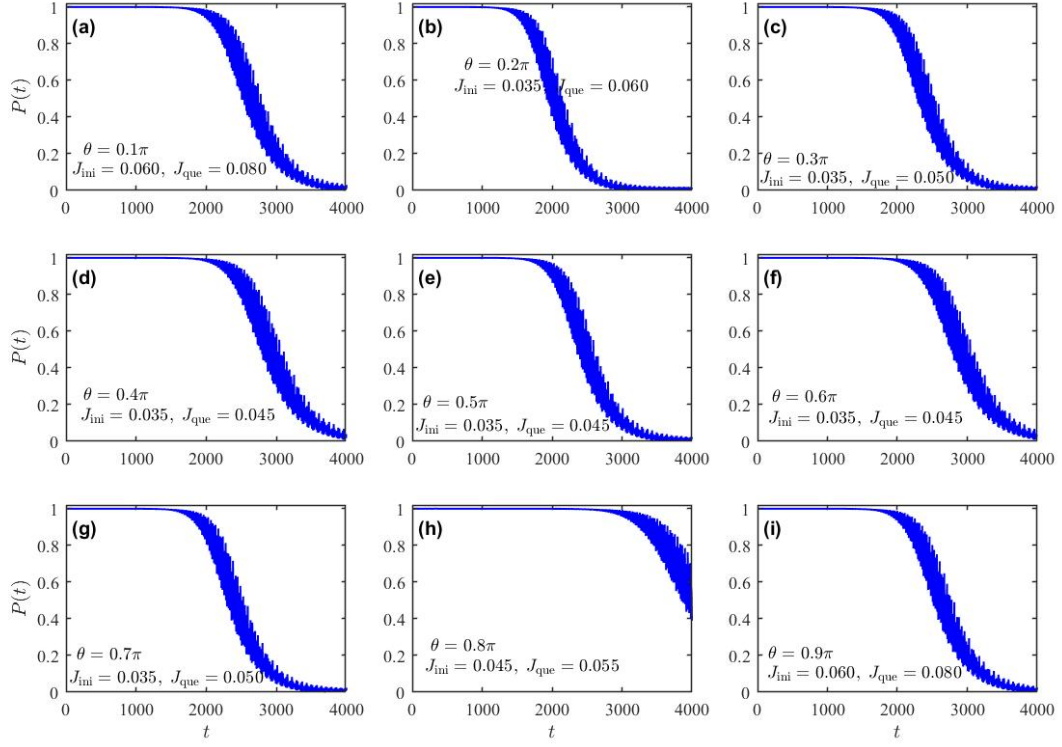


FIG. S8. The quench dynamics around the jump point are always stable at short time. Parameters: $L = 10, N = 2, U = 16, \mu = 4$.